Fundamental Physics and Relativistic Astrophysics with Super Powerful Lasers

S. V. Bulanov

Advanced Photon Research Center,
Japan Atomic Energy Agency, Kizugawa-shi, Kyoto-fu, Japan

Modern Challenges in Nonlinear Plasma Physics
A Conference Honoring the Career of Dennis Papadopolous
June 15-19, Sani, Halkidiki, Greece

3D PIC & EXPERIMENT

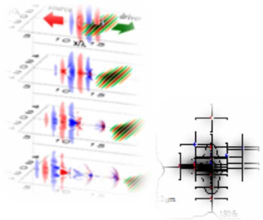

Acknowledgments

M. Borghesi
T. Zh. Esirkepov
D. Habs
I. N. Inovenkov
M. Kando
F. Pegoraro
A. S. Pirozhkov
T. Tajima

OUTLINE

1. Lasers and Astrophysics
2. Shock Waves
3. Reconnection of Magnetic Field Lines & Vortex Patterns
4. Relativistic Rotator
5. Flying Mirror for Femto-, Atto-, … Super Strong Fields
6. Overdense Accelerating Mirror (KAGAMI)
7. Applications
8. Conclusion

1. Lasers and Astrophysics

Morphology of Entities in Space and Laser Plasmas

NIF

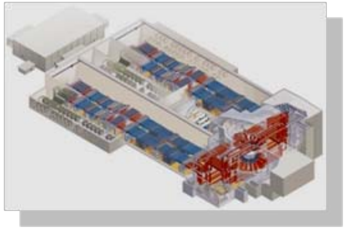

HiPER

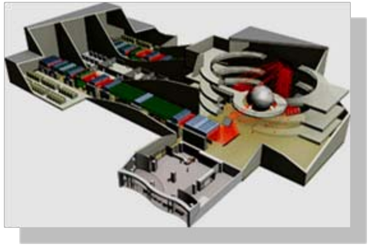

ELI

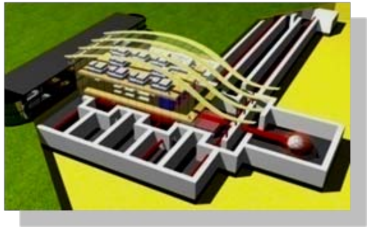

Wake

The Mouse Pulsar

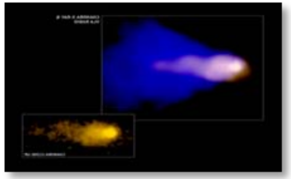

Electron Wake

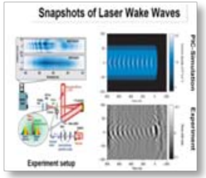

Matlis et al, (2006)

Ion Wake

experiment

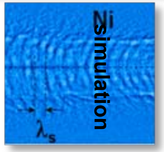

Borghesi, et al, (2005)

Bow Wave

Chandra image of M87

Electron Bow Wave

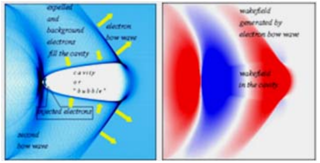

Esirkepov et al (2008)

“Kalmar” Submarine

Photon Bubbles

“Black Widow” pulsar

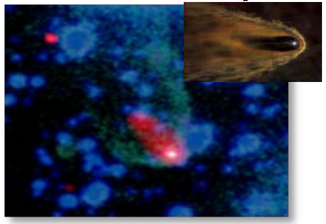

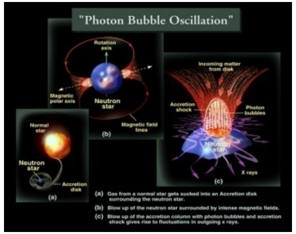

RPDA

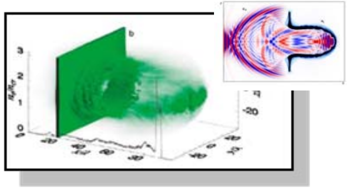

Esirkepov et al (2004)

Lasers

Laser Intensity vs. years

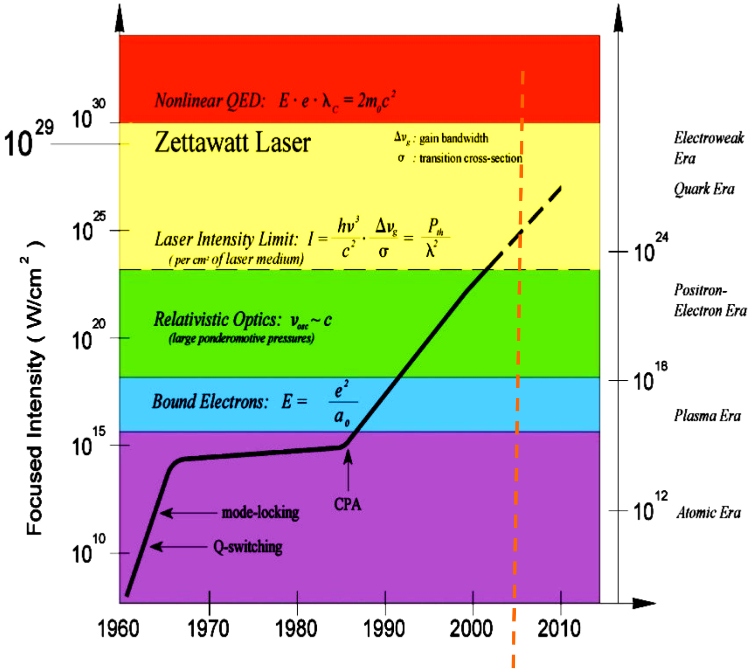

Mourou, G. A., Barty, C. P. J., and Perry, M. D., 1998, Phys. Today 51, 22

CPA

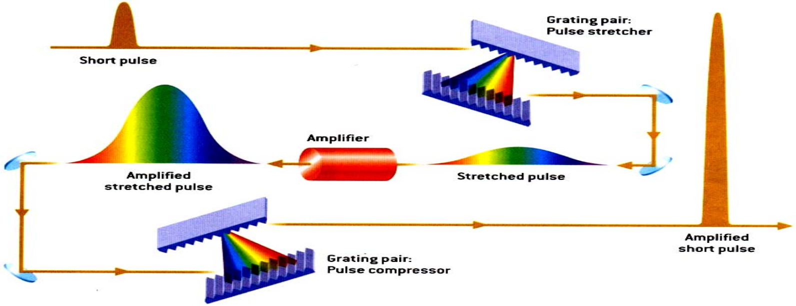

Strickland, D., and Mourou, G., 1986, Opt. Commun. 56, 212.

Relativistic Limit in EM Wave – Plasma Interaction

Quiver energy of electron oscillating in the EM wave with the amplitude E_0 and frequency ω becomes larger than $m_e c^2$ when the dimensionless amplitude of the EM wave is greater than unity:

$$a_0 = \frac{eE_0}{m_e \omega c} > 1$$

In the EM wave interaction with the electron in vacuum its electron energy scales as (Landau & Lifshitz)

$$\mathcal{E} = \frac{1}{2} m_e c^2 a_0^2$$

When the electron oscillates in the EM wave propagating in a plasma we have (Akhiezer & Polovin)

$$\mathcal{E} = m_e c^2 a_0$$

Laser: Condition $a_0 > 1$ corresponds for 1μm laser wavelength to the intensity above 1.35×10^{18} W/cm^2
Today's lasers can provide the intensity $I > 2\times10^{22}$ W/cm^2 , i. e. $a_0 \approx 100$

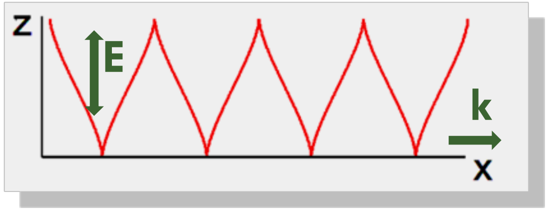

Magneto-dipole Radiation of Oblique Rotator

Space: Magneto-dipole radiation of oblique rotator, has been considered as a model for the pulsar radiation

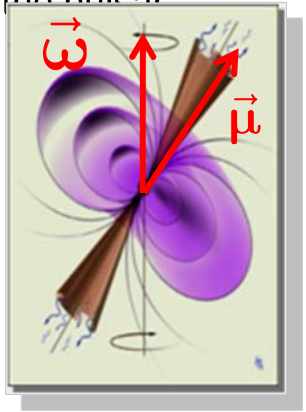

$r = \frac{c}{\omega}$

(Michel; Beskin, Gurevich, Istomin)

Power emitted by rotator is given by $W = \frac{2}{3}\frac{\mu^2 (\sin\theta)^2 \omega^4}{c^3}$

Magnetic moment: $\mu \approx B r_p^3$; θ is the angle between $\vec{\mu}$ and $\vec{\omega}$

The EM wave intensity at the distance r is $I = W/4\pi r^2$

In the wave zone, $r = c/\omega$, the dimensionless wave amplitude is

$$a_0 = \frac{e\mu\omega^2}{m_e c^4}$$

For typical values of magnetic field, $B = 10^{12} G$, rotation frequency, $\omega = 200\, s^{-1}$,

and pulsar radius: $r_p = 10^6 cm$

it yields $a_0 = 10^{10}$

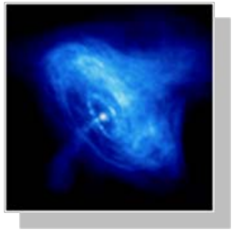

Crab pulsar

Amplitude $\left[a_0 = \frac{eE_0}{m_e c\omega}\right]$	Intensity $\left[\frac{\text{W}}{\text{cm}^2}\right]$	Regime
$a_{QED} = \frac{m_e c^2}{h\omega}$	2.4×10^{29}	e^+, e^- in vacuum
$a_{QM} = \frac{2e^2 m_e c}{3h^2\omega}$	5.6×10^{24}	quantum effects
$a_p = \frac{m_p}{m_e}$	1.3×10^{24}	relativistic p
$a_{rad} = \left(\frac{3\lambda}{4\pi r_e}\right)^{1/3}$	1×10^{23}	radiation damping
$a_{rel} = 1$	1.3×10^{18}	relativistic e^-

SVB, T. Zh. Esirkepov, J. Koga, T. Tajima, 2004

Cross section of nonlinear Thomson scattering

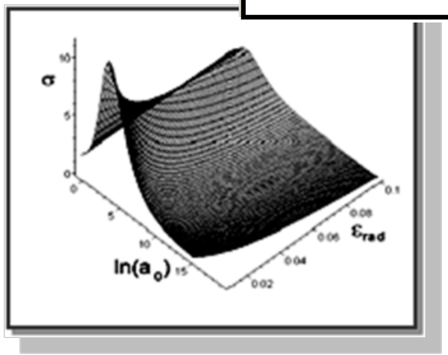

For the Crab pulsar,

$$\omega = 200 s^{-1}, \quad a_0 = 10^{10}$$

the radiation damping effects are crucially important because the EM wave amplitude is above the threshold:

$$a_{rad} = \left(\frac{3\lambda}{4\pi r_e}\right)^{1/3} = 10^7$$

Laboratory Astrophysics

Laboratory Astrophysics

Relativistic Laboratory Astrophysics with the Ultra Short Pulse High Power Lasers

We deal with the collisionless plasmas

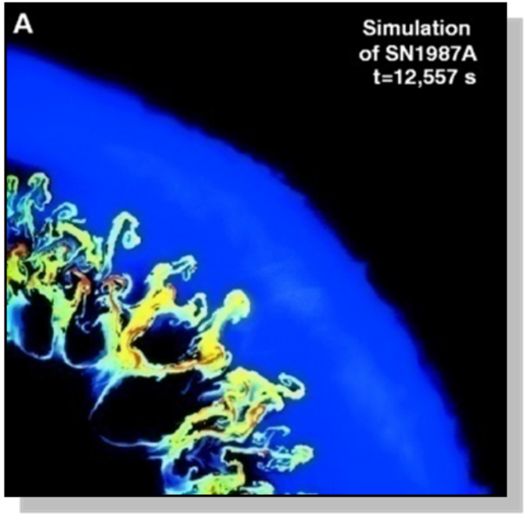

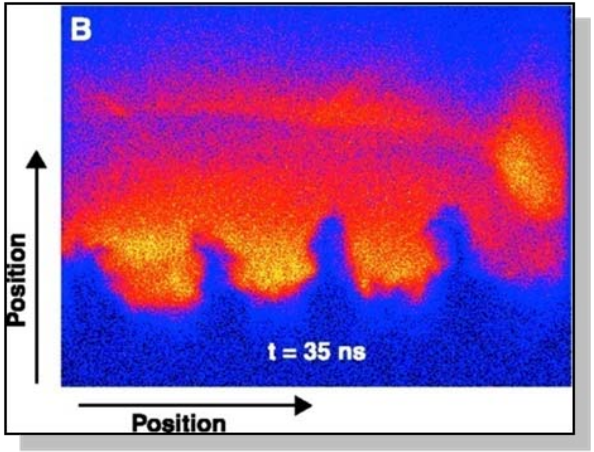

B. A. Remington et al., Science 284, 1488 (1999)

Rayleigh-Taylor & Richtmayer-Meshkov Instability,:
seen in simulations of Supernovae (right) and
in laser irradiated Nuclear Fusion target

Radiative shock waves, plasma jets

Cocoon

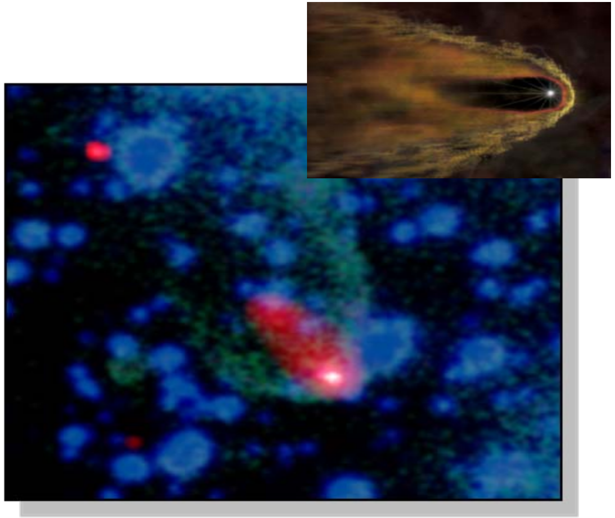

A cocoon around the “black widow” pulsar

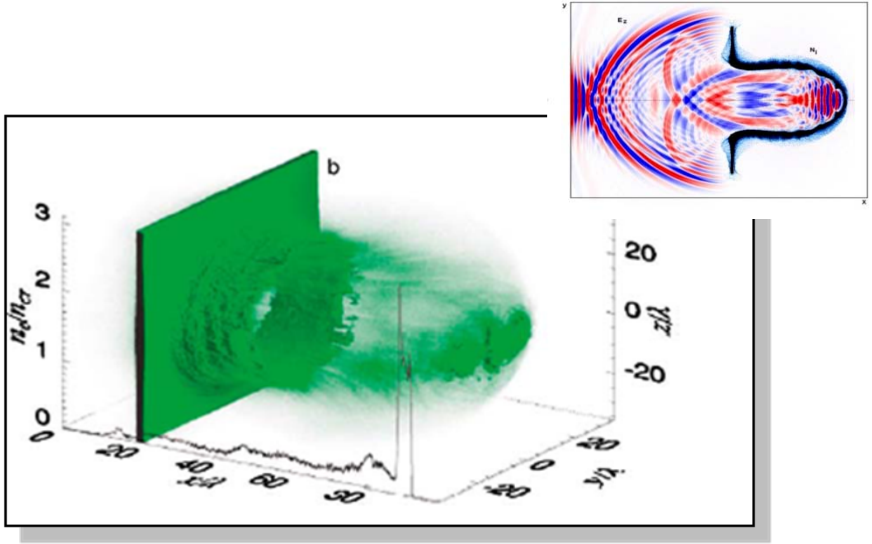

T.Esirkepov, M.Borghesi, SVB, G.Mourou, T.Tajima PRL (2004)

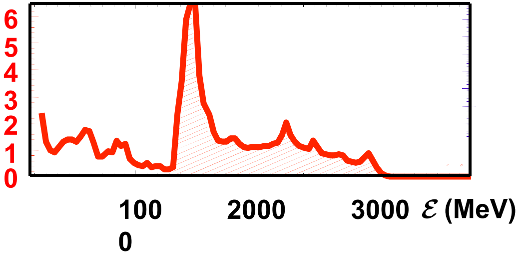

Laser Driven Ion Collider

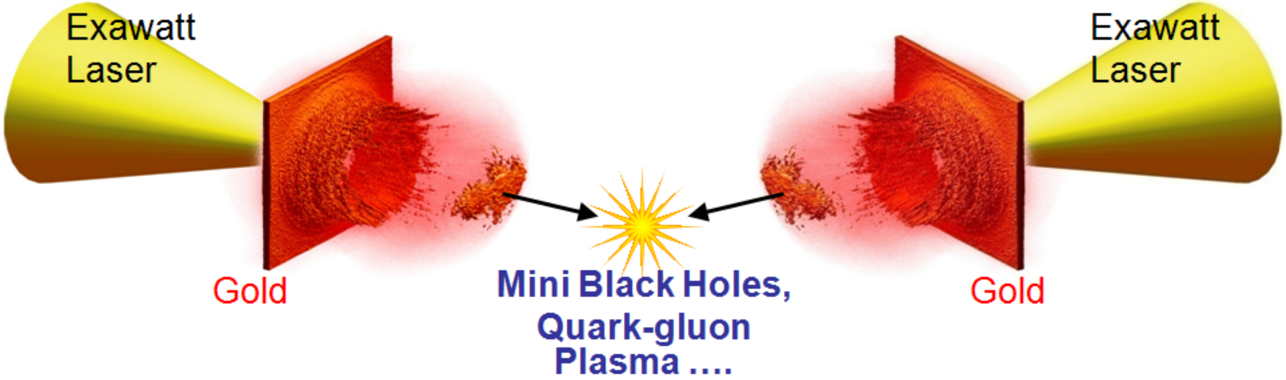

1. Number of events with cross-section σ (for simulation parameters): $\mathcal{N}_{\text{events}} = \sigma N_i^2/S \approx 2\times10^{30}\,\sigma/\text{cm}^2$

2. Acceleration length $l_{acc}=2l_{las}\gamma^2$

   for *1 TeV* and l_{las} *=0.03 cm* it yields l_{acc}*=600 m*

Plasma jets driven by Ultra-intense laser interaction with thin foils

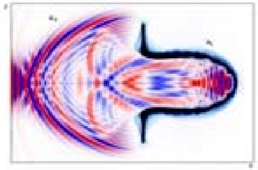

VULCAN Nd-glass laser of Rutherford Appleton laboratory,
(60 J, 1ps & 250 J, 0.7 ps) interacts with foils (3, 5 mum, Al & Cu)

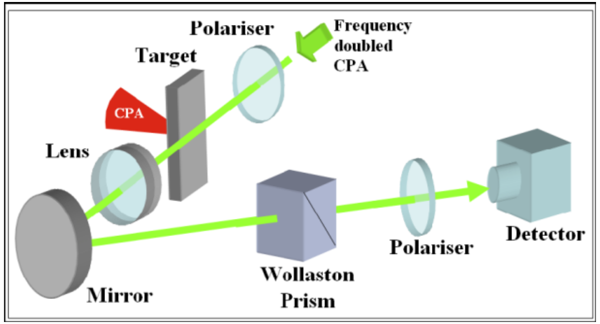

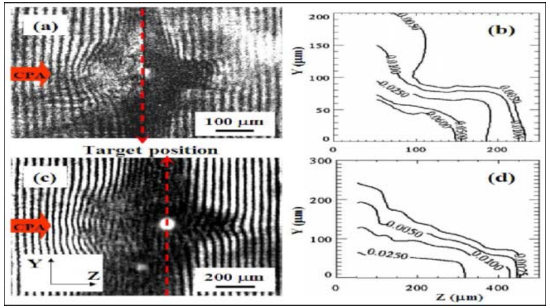

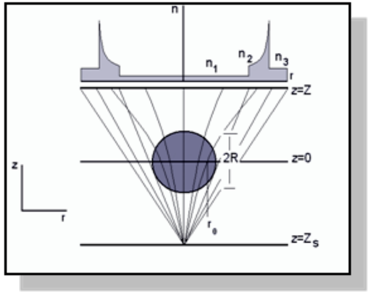

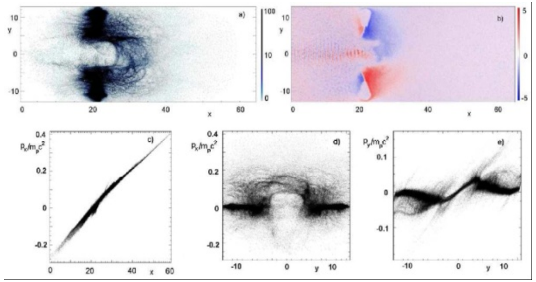

$$\frac{p^{(0)}}{m_p c} = \frac{2W\,(W+1)}{2W+1} \approx 2W$$

$$W = \int \frac{E^2(\psi)}{2\pi n_0 l}\, d\psi \ll 1$$

S. Kar, M. Borghesi, SVB, A.J. Mackinnon, P.K. Patel,
M.H. Key, L. Romagnani, A. Schiavi, A. Macchi, and O. Willi , PRL (2008)

2. Shock Waves

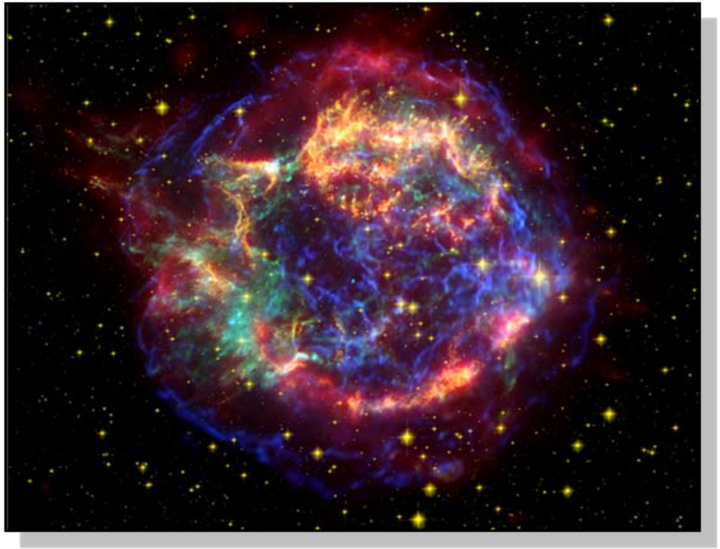

Cassiopea A

Shock Waves and RT Instability

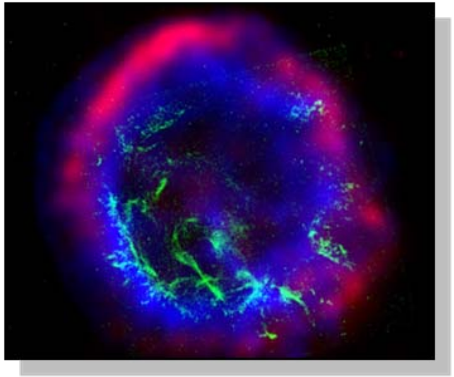

Supernova Remnant E0102-72 from Radio to X-Ray

SN II $\mathcal{E}_{tot} = 10^{52}\,erg$

$1/10 \quad - \quad 1/30 \quad year$

$2\% \quad - \quad 10\%$

TeV gamma sources

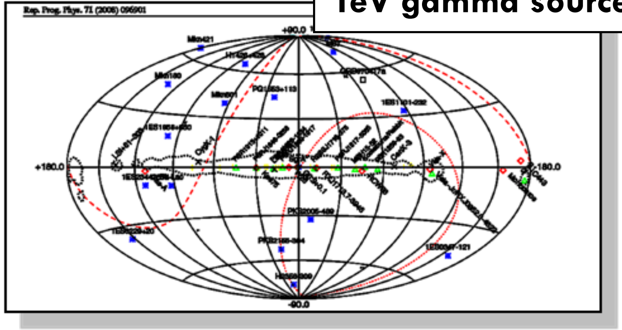

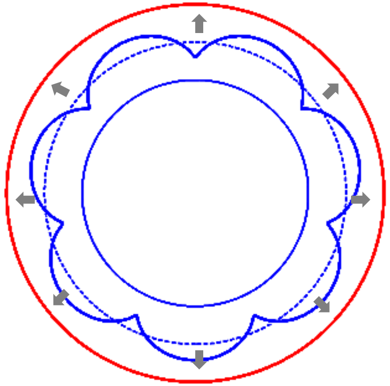

1. Ballistic motion of the ejecta

2. Sedov's regime:

$$R_{SW} = 1.5(\mathcal{E}_{tot} t^2 / \rho)^{1/3} = \frac{5}{2} V_{SW} t$$

$$V_{SW} \propto t^{-3/5}$$

3. Radiation losses: $R_{SW} \propto t^{2/7}$

Acceleration at the Shock Wave Front

CR have a power law energy spectrum over several orders of magnitude energy range

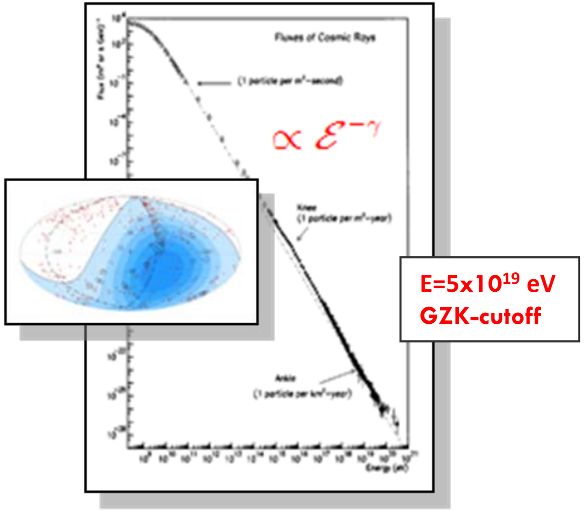

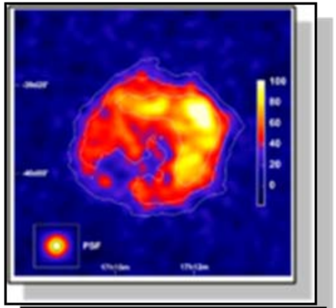

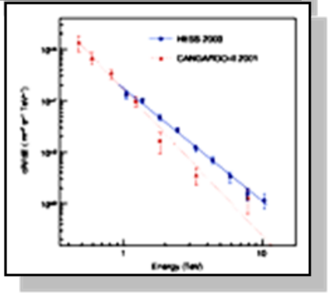

The gamma ray image of RX J1713.7-3946 spectrum and gamma ray obtained with the HESS telescope array (Aharonyan et al, 2008)

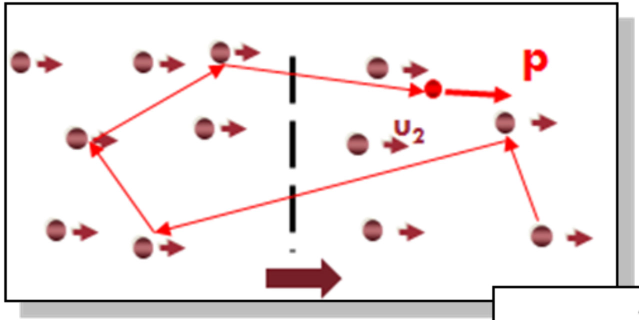

"Fermi acceleration"
G.F. Krymskii (1977)

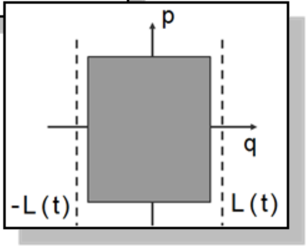

$$\frac{\partial}{\partial x}\left(u(x)\, f - D\frac{\partial f}{\partial x}\right) = -\frac{2u_1}{3(\kappa+1)}\delta(x)\frac{1}{p^2}\frac{\partial}{\partial p}\left(p^2 f\right)$$

$$pL = const$$

$$u_2 = \frac{\kappa-1}{\kappa+1}u_1$$

$$u_1 > u_2$$

$$f(p) = Cp^{-\gamma}$$

$$\gamma = \frac{3u_1}{u_1 - u_2}$$

Collisionless Shock Waves

A structure of collisionless schock waves is determined by the counter play of dissipation and dispersion effects. These effects are described within the framework of the Korteweg-de Veries-Burgers equation:

$$\partial_t u + u\partial_x u - \nu\,\partial_{xx} u - \beta\,\partial_{xxx} u = 0$$

nonlinearity dispersion

dissipation

R.Z.Sagdeev, 1959

a) MS wave propagating almost perpendicularly to B field $\beta \approx v_a c^2 / 2\omega_{pe}$

with $v_a = B^2 / \sqrt{4\pi n m_p}$

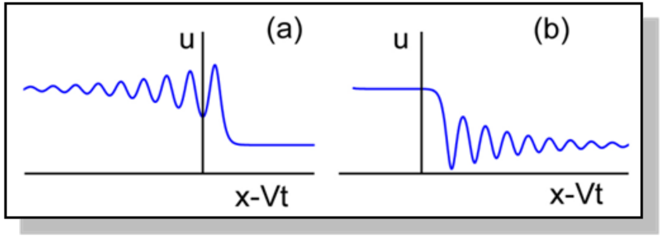

b) MS wave propagation is almost parallel to B field

$\beta \approx -v_a c^2 / 2\omega_{pe}$

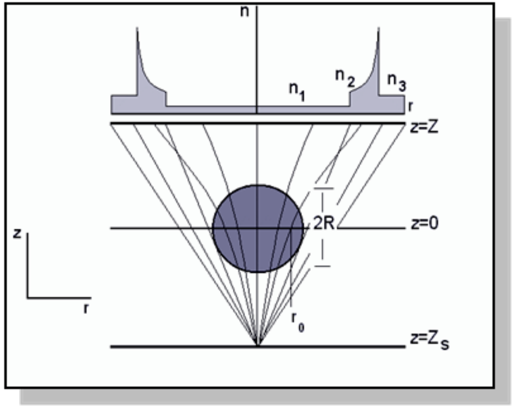

Observation of Collisionless Shocks in Laser-Plasma Experiments

L. Romagnani,[1,*] S. V. Bulanov,[2,3] M. Borghesi,[1] P. Audebert,[4] J. C. Gauthier,[5] K. Löwenbrück,[6] A. J. Mackinnon,[7] P. Patel,[7] G. Pretzler,[6] T. Toncian,[6] and O. Willi[6]

[1]*School of Mathematics and Physics, The Queen's University of Belfast, Belfast, Northern Ireland, United Kingdom*
[2]*APRC, JAEA, Kizugawa, Kyoto, 619-0215 Japan*
[3]*Prokhorov Institute of General Physics RAS, Moscow, 119991 Russia*
[4]*Laboratoire pour l'Utilisation des Lasers Intenses (LULI), UMR 7605 CNRS-CEA-École Polytechnique-Univ. Paris VI, 91128 Palaiseau, France*
[5]*Université Bordeaux 1; CNRS; CEA, Centre Lasers Intenses et Applications, 33405 Talence, France*
[6]*Institut für Laser–und Plasmaphysik, Heinrich-Heine-Universität, Düsseldorf, Germany*
[7]*Lawrence Livermore National Laboratory, Livermore, California 94550, USA*

(Received 4 April 2008; published 10 July 2008)

The propagation in a rarefied plasma ($n_e \lesssim 10^{15}$ cm^{-3}) of collisionless shock waves and ion-acoustic solitons, excited following the interaction of a long ($\tau_L \sim 470$ ps) and intense ($I \sim 10^{15}$ W cm^{-2}) laser pulse with solid targets, has been investigated via proton probing techniques. The shocks' structures and related electric field distributions were reconstructed with high spatial and temporal resolution. The experimental results were interpreted within the framework of the nonlinear wave description based on the Korteweg–de Vries–Burgers equation.

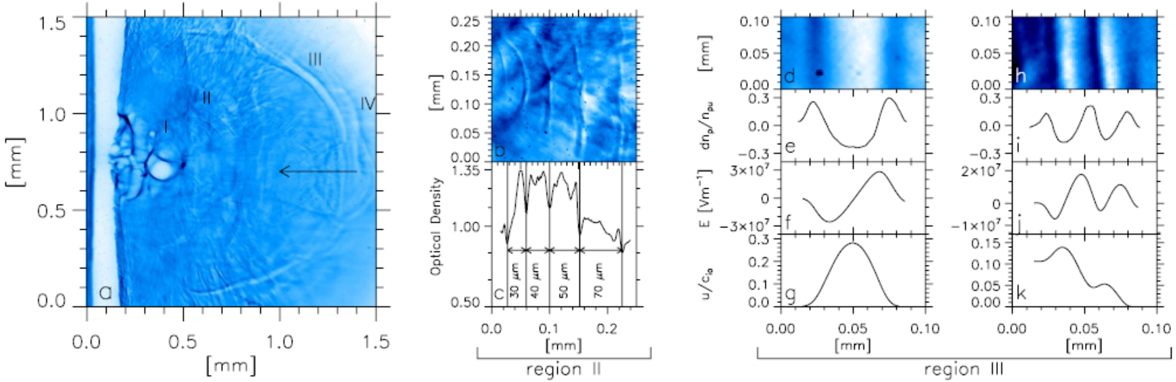

Soliton **Shock Wave**

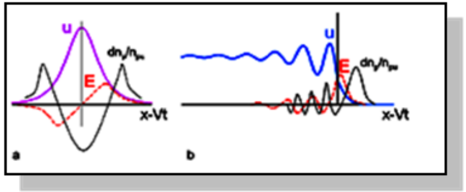

3. Reconnection of Magnetic Field Lines & Vortex Patterns

Solar Flare

Von Karman vortex row made by the wind over the Pacific island of Guadalupe

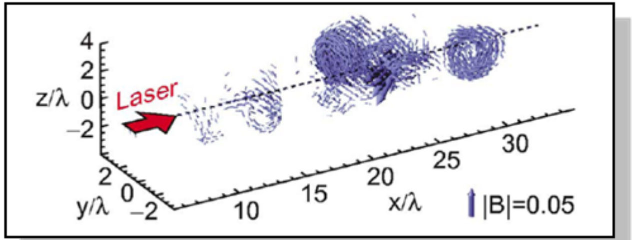

Magnetic (vortex) wake behind the laser pulse: Esirkepov, et al., 2004

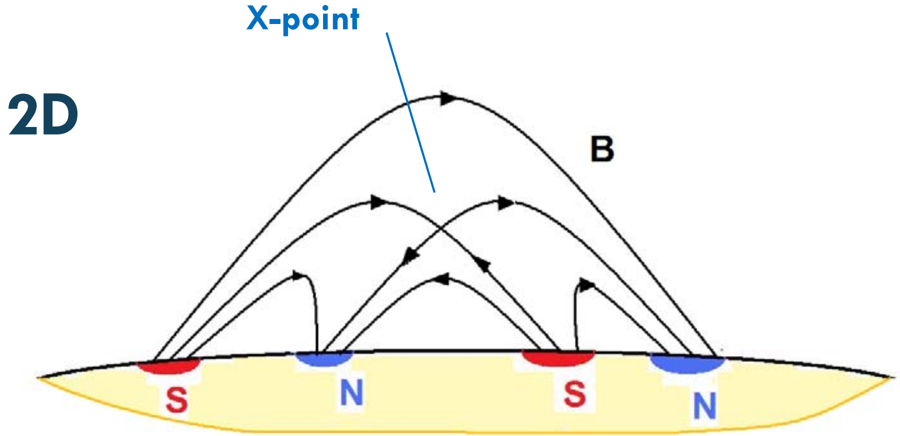

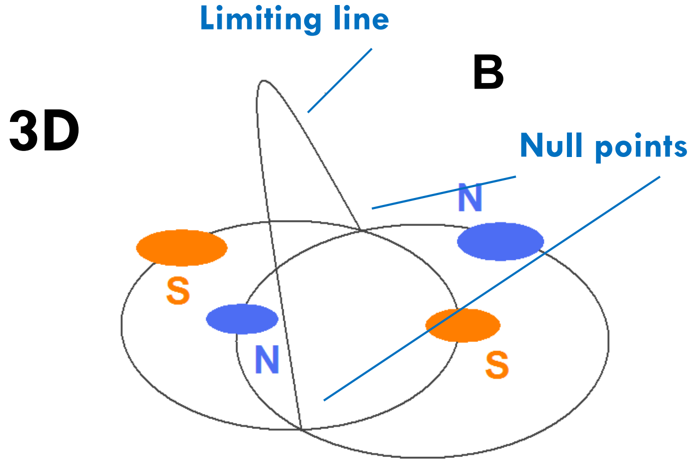

Sweet (1965)

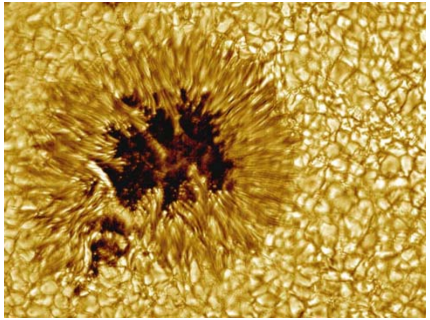

Sunspot

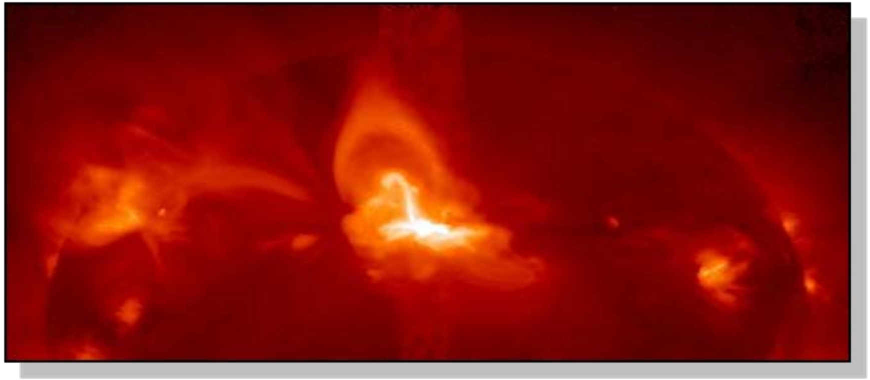

Solar Flare

Local Structure of the Magnetic Field

Near null point we can expand the magnetic field as

$$\mathbf{B}(\mathbf{x},t) = (\mathbf{B}(0,t)\nabla)\mathbf{x} + \dots .$$

Introducing the matrix $\partial B_i / \partial x_j \big|_{x=0} = A_{ij}, \quad B_i = A_{ij} x_j$

we write for the magnetic field lines $\dfrac{dx_i}{ds} = A_{ij} x_j .$

It yields $\det\left(A_{ij} - \lambda \delta_{ij}\right) = 0,$

The topology is determined by the eigenvalues $\lambda_\alpha \quad \left(\sum_\alpha \lambda_\alpha = 0\right)$

We have the null surface, null line or null point depending on

$$\lambda_{1,2} = \pm\lambda' \text{ or } \lambda_{1,2} = \pm i\lambda'' \qquad \lambda_3 = 0$$

$$\lambda_{1,2} = \lambda' \pm i\lambda'' \qquad \lambda_3 = \lambda'$$

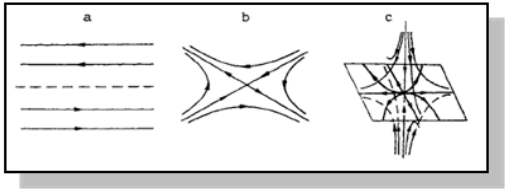

SVB, M. A.Ol'shanetskij (1983)

Self-similar plasma motion near 3D critical points

The Euler x_i and the Lagrange x_i^0 coordinates

$$v_i(x,t) = w_{ij}(t)x_j, \quad B_i(x,t) = A_{ij}(t)x_j, \quad x_i = M_{ij}(t)x_j^0$$

From the MHD equations we have

$$\rho = \rho_0 / D, \quad A_{ij}(t) = M_{ik}A_{kl}(0)M_{lj}^{-1} / D, \quad w_{ij} = \dot{M}_{ik}M_{kj}^{-1}, \quad D = \det\{M_{ij}\}$$

$$\ddot{M}_{ik} = \frac{1}{4\pi\rho_0 D}\left(M_{ik}A_{kl}^0 A_{lj}^0 - M_{sk}A_{kl}^0 M_{lt}^{-1} M_{st} A_{tj}^0\right)$$

The singularity (magnetic collapse) appears in a finite time at $t \to t_0$

$$w_{ij} \propto (t_0 - t)^{-1}, \quad A_{ij} \propto (t_0 - t)^{-4/3}$$

SVB & M.Ol'shanetskij, 1984

3 D Magnetic Collapse near 3D Null Point (Lagrange Surfaces versus Time)

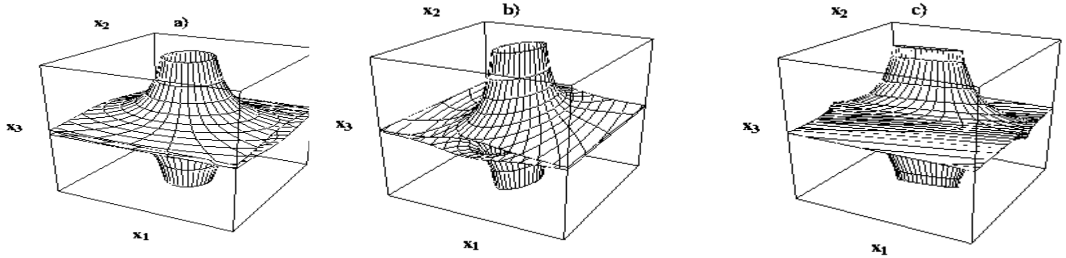

The electric current is perpendicular to the separatrix surface

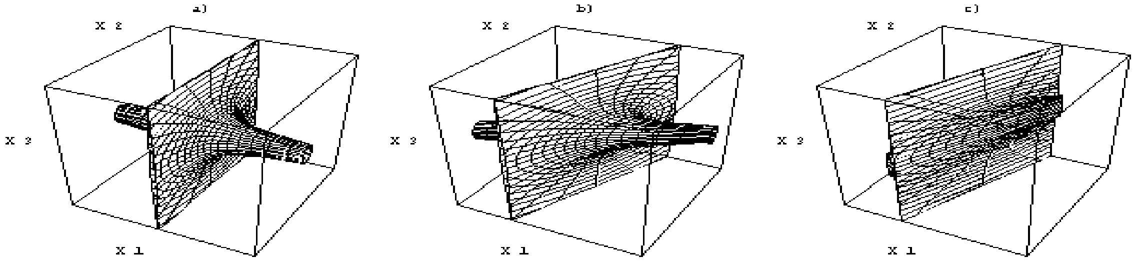

The electric current is parallel to the separatrix surface

2D: V.S.Imshennik & S.I.Syrovatskii, (1967)

3D: SVB & M.Ol'shanetskij (1984); SVB&J.-I.Sakai(1997)

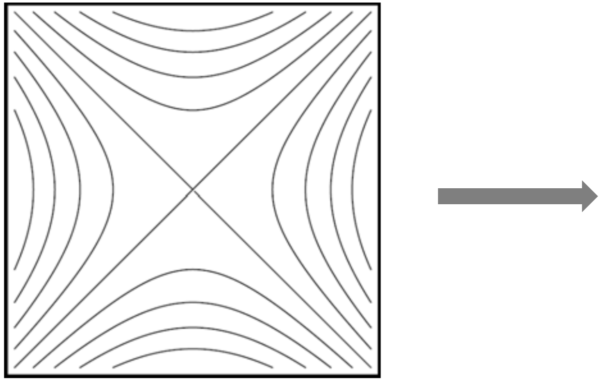

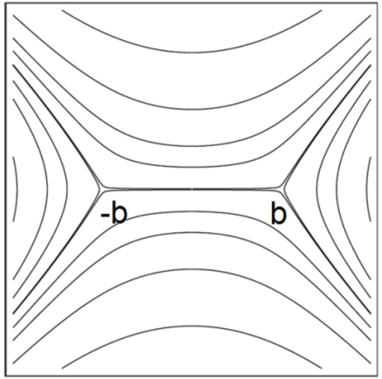

S. I. Syrovatskii, 1971

$$b = \sqrt{4I/hc}$$

$$\Phi = h\varsigma^2/2$$

$$\Phi = h\left[\varsigma\sqrt{\varsigma^2 - b^2} - \mathrm{Ln}\left(\varsigma - \sqrt{\varsigma^2 - b^2}\right)\right]$$

Current sheet near the X-line
of magnetic configuration

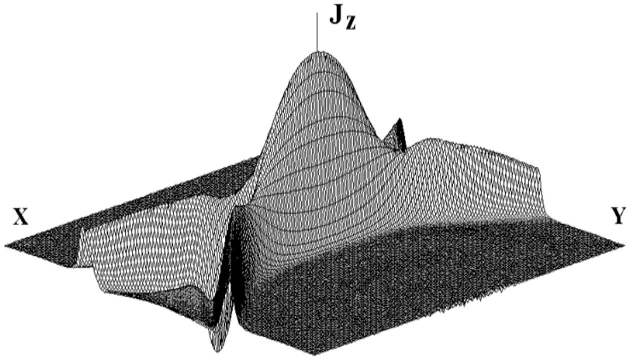

SVB, et al, 1996

Reconnection of Magnetic Field Lines

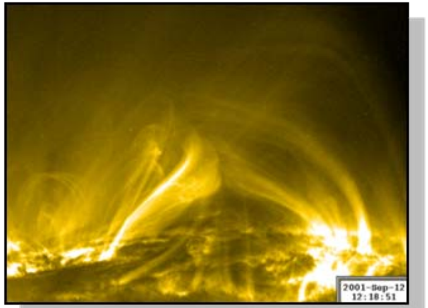

Solar flare/
12.09.2001(12:18:51)

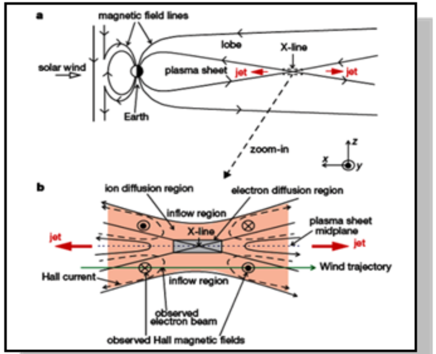

M. Oieroset, et al.,
Nature (2001)

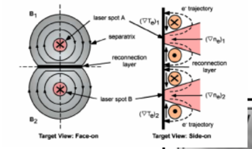

B.Coppi et al (1965)

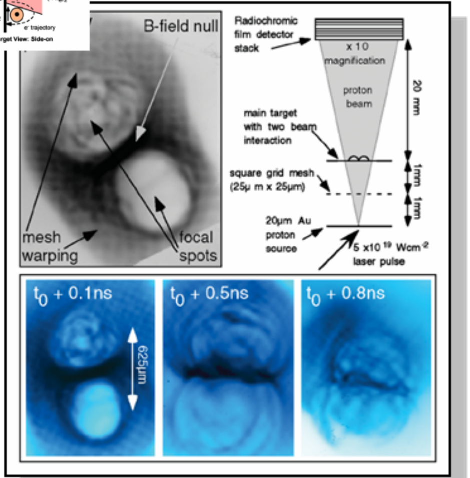

Nilson et al, PRL 97, 255001 (2006)

MAGNETIC RECONNECTION IN LASER PLASMAS HAS BEEN FORESEEN IN:

G.A.Askar'yan, SVB, F.Pegoraro, A.M.Pukhov,
Magnetic interaction of self-focused channels and magnetic wake excitation in high intense laser pulses,
Comments on Plasma Physics and Controlled Fusion 17, 35 (1995).

Magnetic Reconnection in Collisionless Plasmas

In collisionless multispecies plasmas the **curl** of the canonical momentum

$$\mathbf{p}_\alpha = m_\alpha \mathbf{v}_\alpha + (e_\alpha / c)\mathbf{A}$$

is frozen in the corresponding flow velocity

$$\partial_t \nabla \times \mathbf{p}_\alpha = \nabla \times \left[\mathbf{v}_\alpha \times \nabla \times \mathbf{p}_\alpha\right]$$

The electron magnetohydrodynamics considers the dynamics of just the electrons, the ions are assumed to be at rest and the quasineutrality condition is fulfilled. The electron velocity is related to the magnetic field as

$$\mathbf{v}_e = -(c / 4\pi n_e)\nabla \times \mathbf{B}$$

with constant plasma density $n_e = n_i$. It yields

$$\partial_\mathbf{t}(\mathbf{B} - \Delta \mathbf{B}) = \nabla \times [(\nabla \times \mathbf{B}) \times (\mathbf{B} - \Delta \mathbf{B})]$$

In the linear approximation EMHD describes the whistler waves

The EMHD equations can be written as

$$\partial_t \mathbf{\Omega} = \nabla \times [(\nabla \times \mathbf{B}) \times \mathbf{\Omega}]$$

Here the generalized vorticity

$$\mathbf{\Omega} = \mathbf{B} - \Delta\mathbf{B} = \nabla \times (\mathbf{A} - \Delta\mathbf{A}) = \mathbf{B} + \nabla \times \mathbf{v}$$

is frozen into the electron fluid motion.

We consider the magnetic field given by

$$\mathbf{B} = \nabla \times (A_{||}\mathbf{e}_z) + B_{||}\mathbf{e}_z$$

The magnetic field pattern in the x , y plane is determined by

$$A_{||}(x, y, t) = const$$

Magnetic field

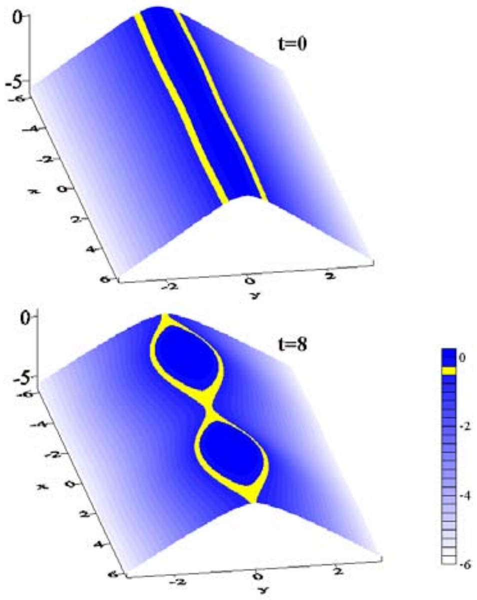

$A_{||} = \mathrm{const}$

Generalized vorticity

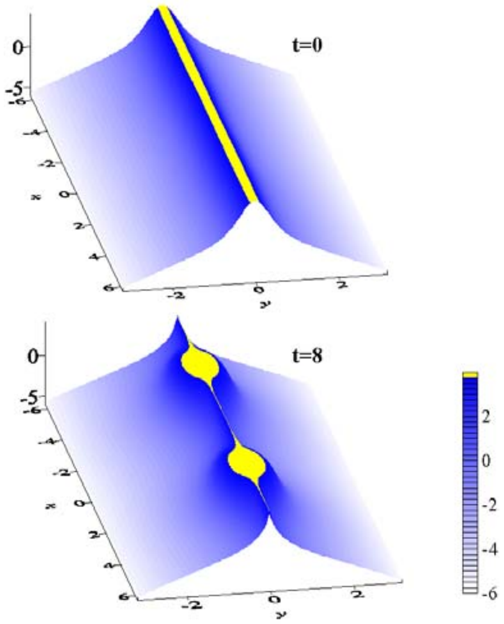

$A_{||} - \Delta A_{||} = \mathrm{const}$

K.Avinash, SVB, T.Esirkepov, P.Kaw, F.Pegoraro, P.Sasorov, A.Sen,
Forced Magnetic Field Line Reconnection in Electron Magnetohydrodynamics.
***Physics of Plasmas* 5, 2946 (1998)**

Charged Particle Acceleration

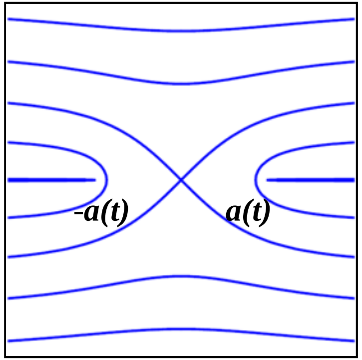

In the vicinity of the X-line, the magnetic field is described by

$$B(\varsigma,t) = B_0 \frac{\varsigma}{\sqrt{a^2(t)-\varsigma^2}} \approx B_0 \frac{\varsigma}{a(t)}$$

$$\Phi(\varsigma,t) = B_0\sqrt{a^2(t)-\varsigma^2}$$

and the electric field is given by

$$E(\varsigma,t) = -B_0 \frac{a(t)\dot{a}(t)}{c\sqrt{a^2(t)-\varsigma^2}} \approx \frac{\dot{a}(t)}{c} B_0$$

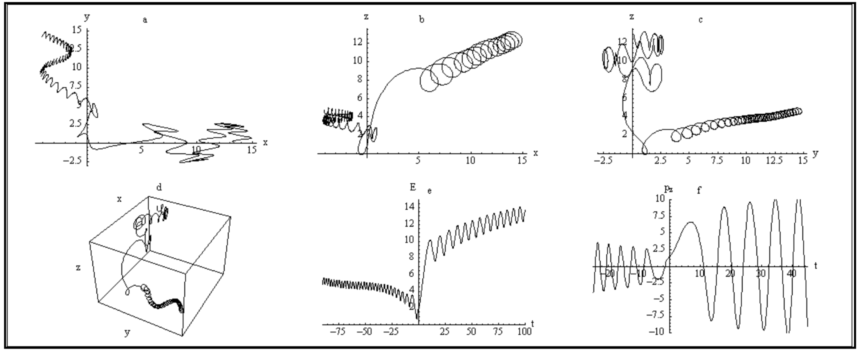

The energy spectrum of fast particles is given by

$$\frac{d\mathcal{N}(\mathcal{E})}{d\mathcal{E}} \propto \exp\left(-\sqrt{\frac{2\mathcal{E}}{m\dot{a}^2}}\right)$$

SVB, Sasorov; SVB, Cap

Electron Vortices behind the Laser Pulse

Antisymmetric vortex row

$B_z(x, y)$

$n_i(x, y)$

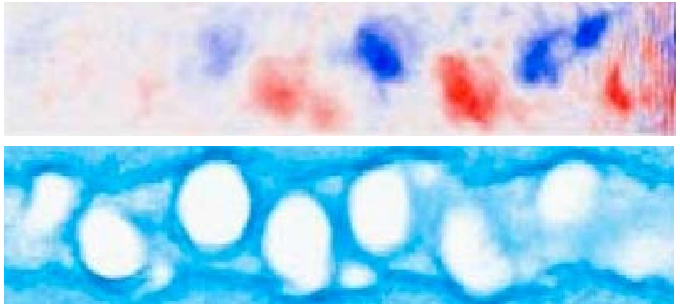

L.M.Chen et al., Phys. Plasmas, 14, 040703 (2007)

Von Karman vortex row
H.Lamb, Hydrodynamics, 1947

Vortices described by the Hasegawa-Mima equation

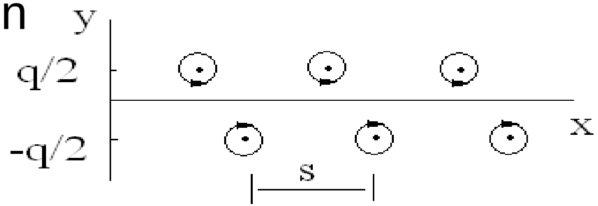

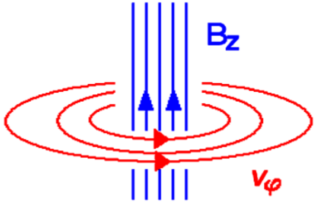

Electron vortex

SVB, T.Esirkepov, M.Lontano, F.Pegoraro,A.Pukhov, Phys. Rev. Letts. 76, 3562 (1996).

Interacting Point Vortices

As we know $\nabla \times (\mathbf{p} - e\mathbf{A}/c)$ is frozen:

$$(\partial_t + \mathbf{e}_z \times \nabla B \cdot \nabla)(\Delta B - B) = 0$$

Discret vortices are described by equation $\Omega = \Delta B - B = \sum_j \Gamma_j \delta(\mathbf{r} - \mathbf{r}_j(t))$

its solution gives for the magnetic field $B = \sum_j B_j(\mathbf{r}, \mathbf{r}_j(t)) = -\sum_j \frac{\Gamma_j}{2\pi} K_0(|\mathbf{r} - \mathbf{r}_j(t)|)$

and the velocity of j-th vortex is

$$\frac{d\mathbf{r}_j}{dt} = \mathbf{e}_z \times \nabla \sum_{k \neq j} B_k(\mathbf{r}_j(t), \mathbf{r}_k(t)) \Longleftrightarrow \begin{cases} \dfrac{dx_j}{dt} = \dfrac{1}{2\pi} \sum_{k \neq j} \Gamma_k \dfrac{y_k - y_j}{|\mathbf{r}_j(t) - \mathbf{r}_k(t)|} K_1(|\mathbf{r}_j(t) - \mathbf{r}_k(t)|) \\ \dfrac{dy_j}{dt} = \dfrac{1}{2\pi} \sum_{k \neq j} \Gamma_k \dfrac{x_j - x_k}{|\mathbf{r}_j(t) - \mathbf{r}_k(t)|} K_1(|\mathbf{r}_j(t) - \mathbf{r}_k(t)|) \end{cases}$$

The Hamilton equations

Domain of Stability

Antisymmetric vortex row

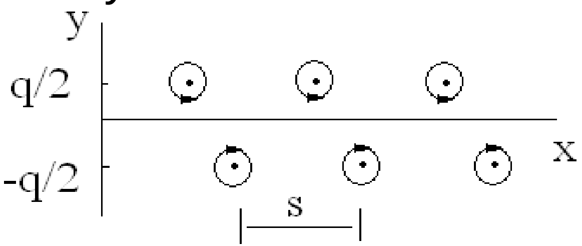

Lyapunov stability in the stability domain was proved

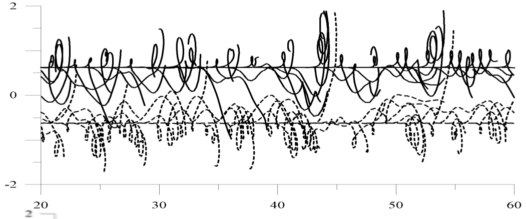

unstable

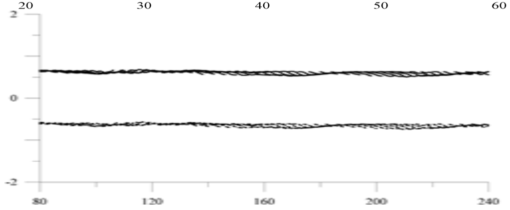

stable

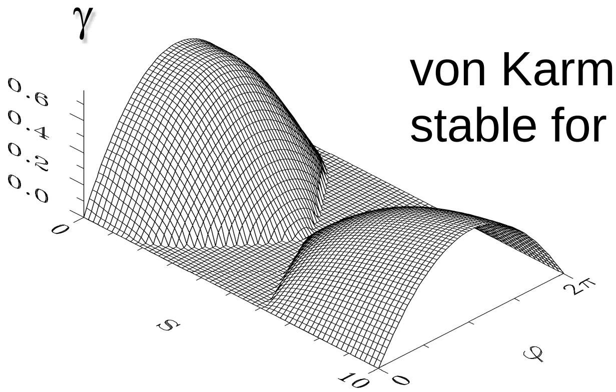

von Karman row is stable for q/s=0.281

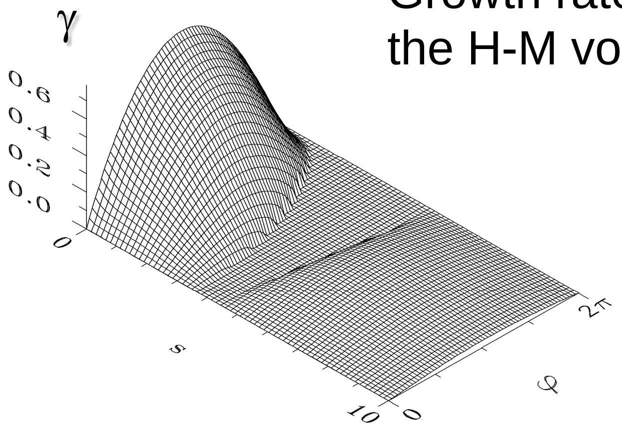

Growth rate vs q and s for the H-M vortex row

Experimental Observations

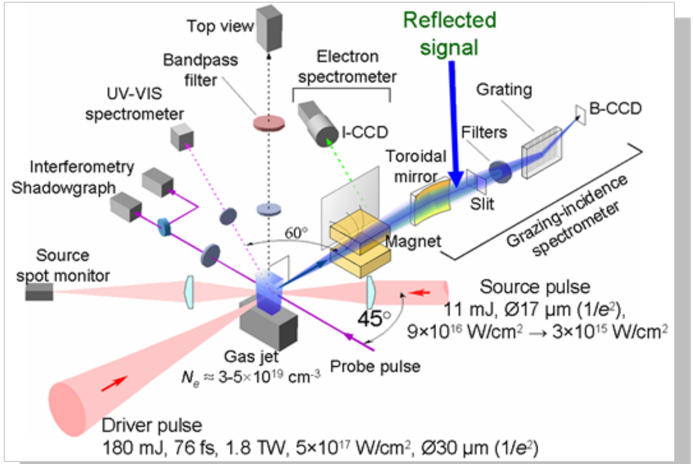

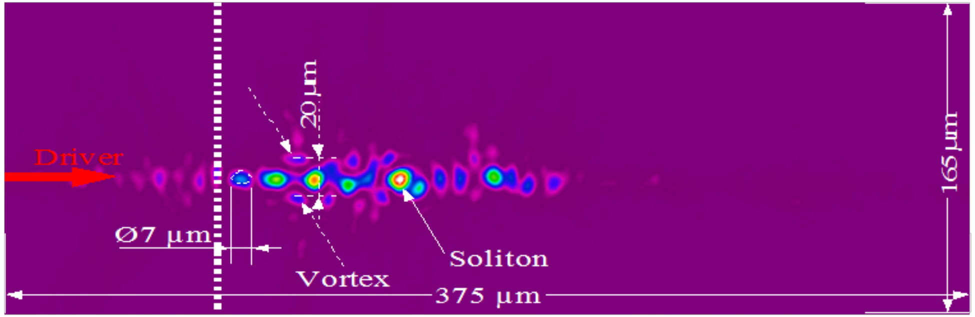

side view

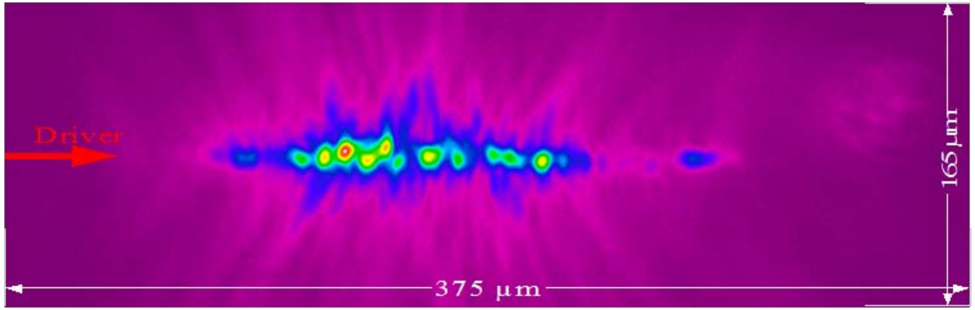

Top view

4. Relativistic Rotator

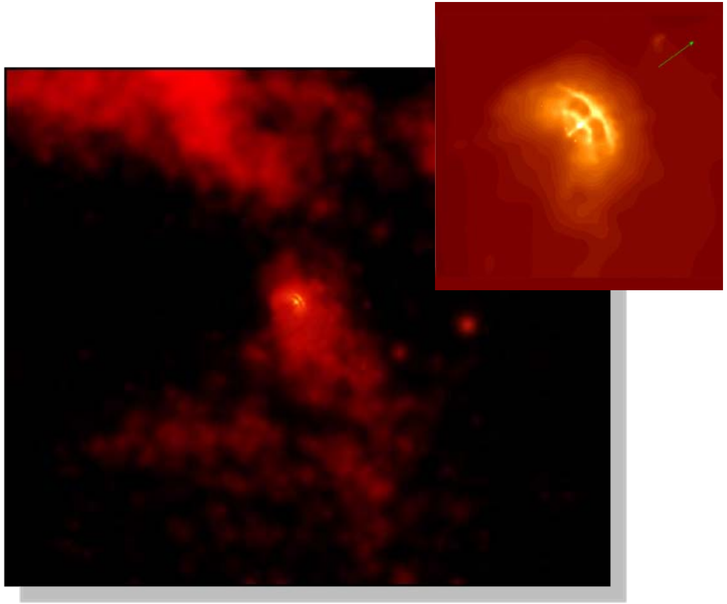

PeV γ from Crab Nebula

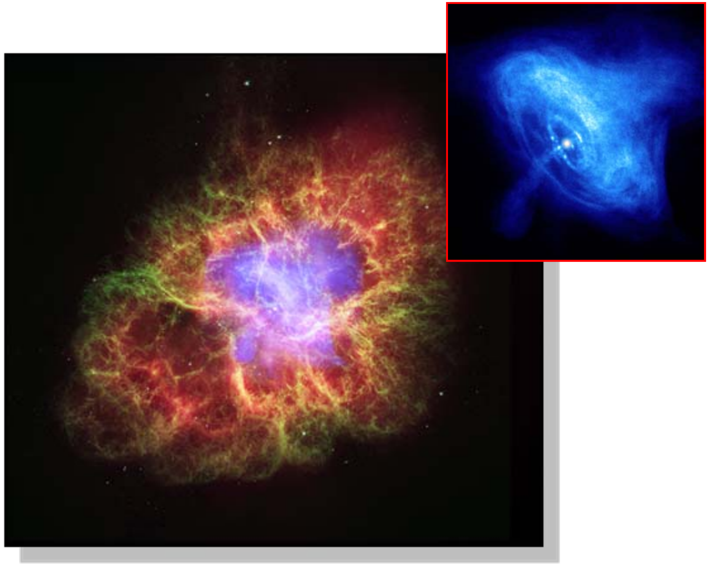

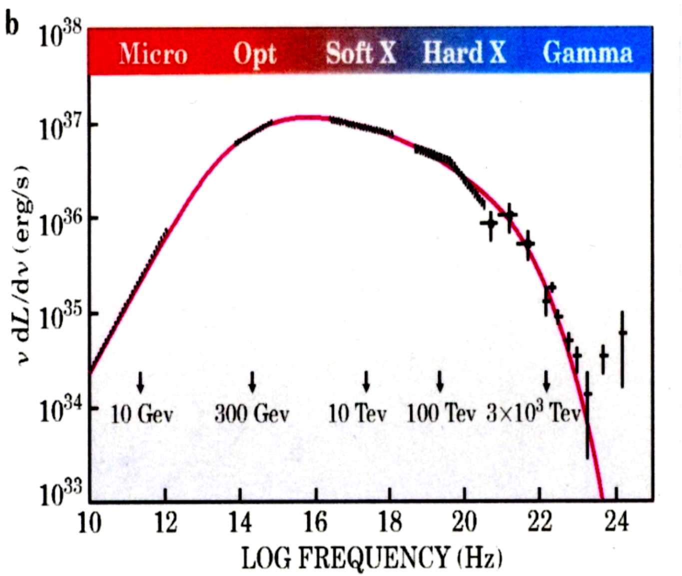

The Crab Pulsar, lies at the center of the Crab Nebula. The picture combines optical data (red) from the Hubble Space Telescope and x-ray images (blue) from the Chandra Observatory. The pulsar powers the x-ray and optical emission, accelerating charged particles and producing the x-rays.

ON THE PULSAR EMISSION MECHANISMS

1975

V. L. Ginzburg
P. N. Lebedev Physical Institute, Academy of Sciences of the USSR, Moscow, USSR

V. V. Zheleznyakov
Radio-Physical Institute, Gorkii, USSR

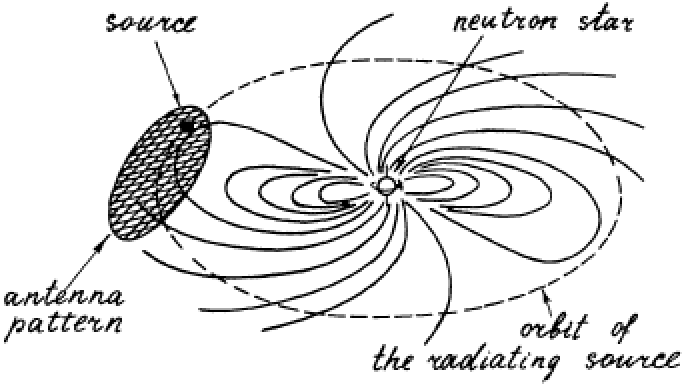

Figure 2 Schematic pulsar model.

RELATIVISTIC E.M. SOLITONS

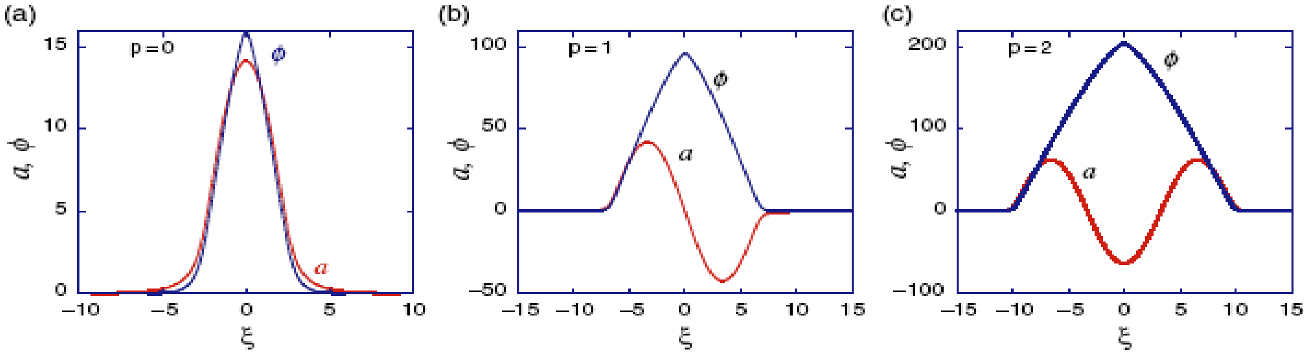

Potential waveforms for bright solitons with $p = 0, 1, 2$ and velocities close to breaking.

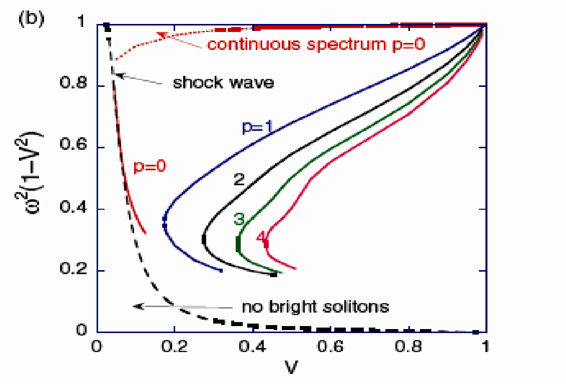

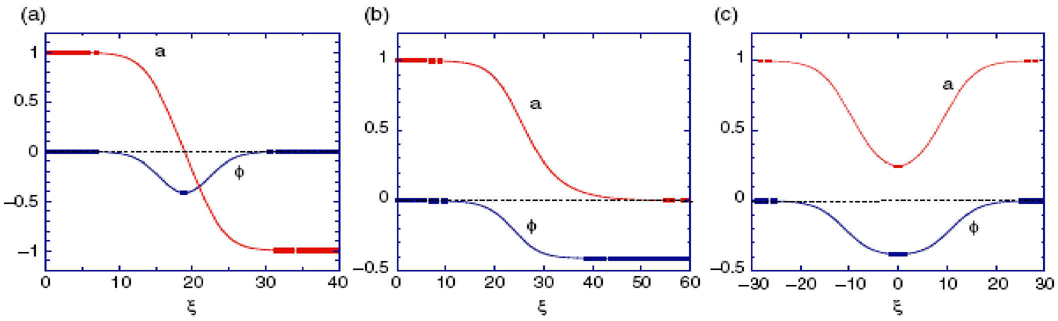

Waveforms of a black soliton (a), a shock wave (b) and a grey soliton (c).

D. Farina, S. Bulanov, Phys. Rev. Lett. 86, 5289 (2001)

Relativistic EM Soliton

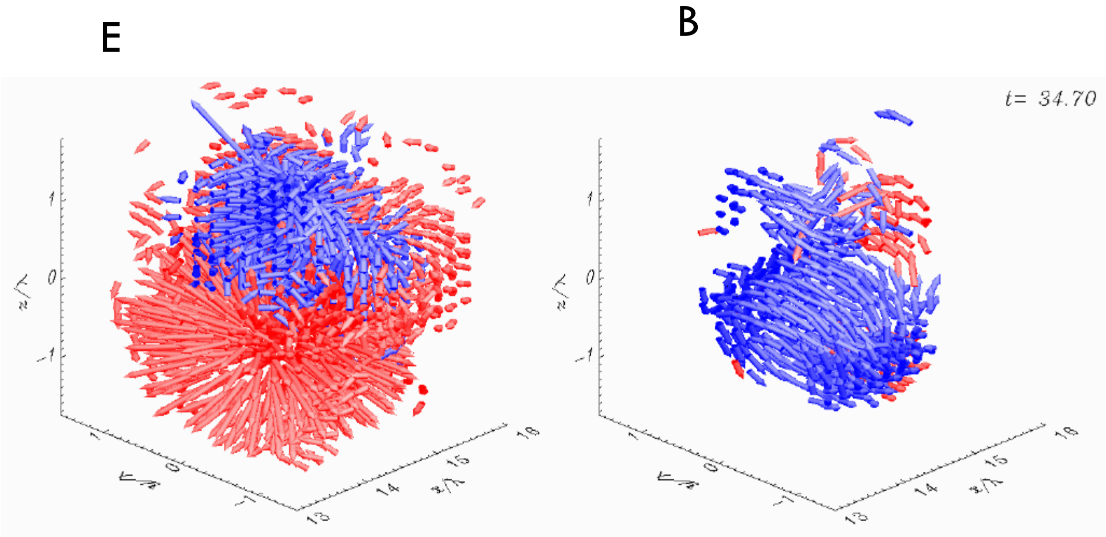

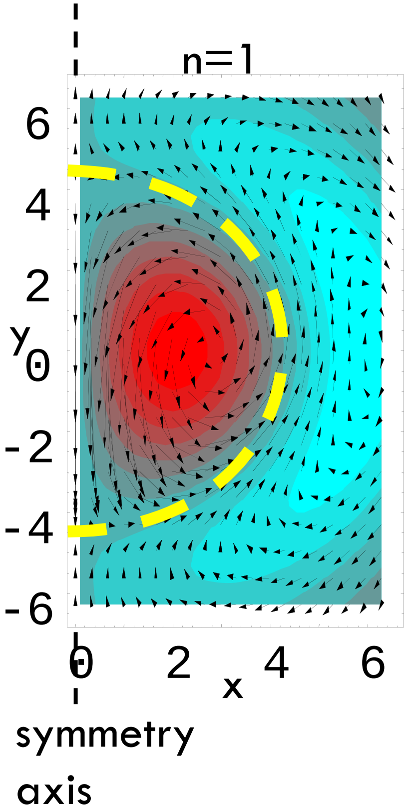

E.M. field in a spherical resonator

T.Esirkepov, SVB, K.Nishihara, F.Pegoraro, PRL (2003)

Macroscopic Evidence of Soliton Formation in Laser-Plasma Interaction

M.Borghesi et al, Phys. Rev. Lett. 88, 135002 (2002)

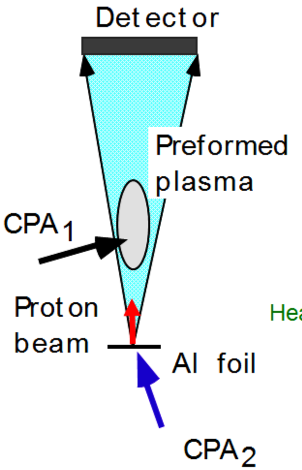

VULCAN laser, RAL

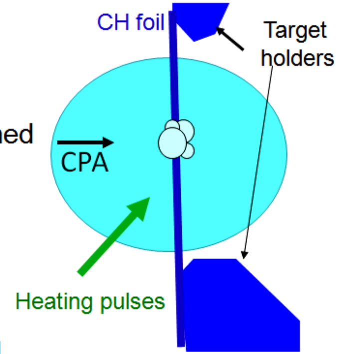

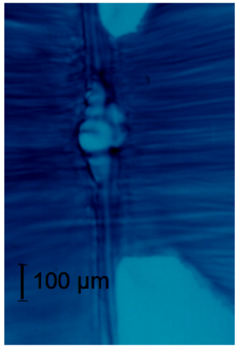

Underdense plasma (n_{peak}~0.1-0.2 n_c)

I~ 10^{19} W/cm^2, probing: +45 ps

"Bubbles" observed only after the interaction. They die out after 60-80 ps

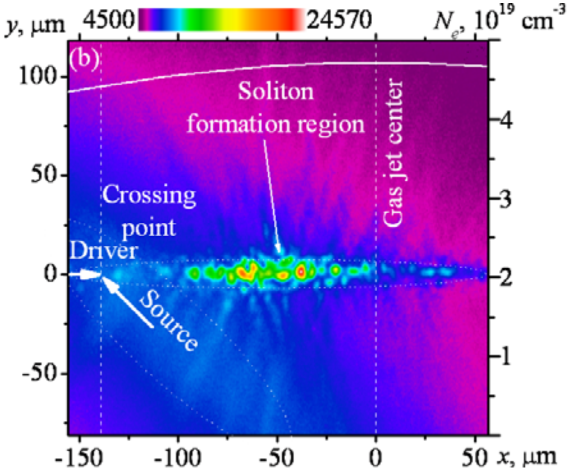

A.S.Pirozhkov et al., Phys.Plasmas, 14, 123106 (2007)

Circularly Polarized Soliton (3D PIC)

$B_z(x,y)$

$n_e(x,y)$

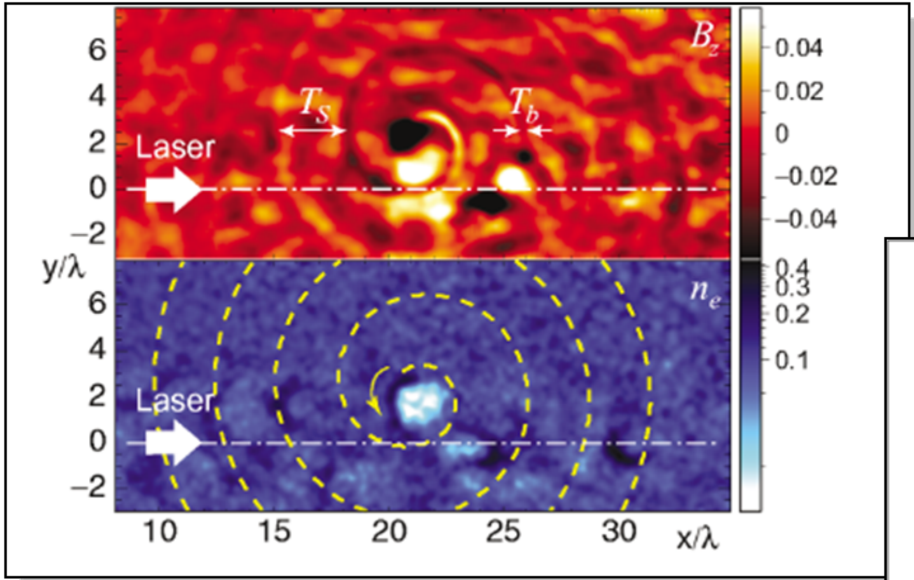

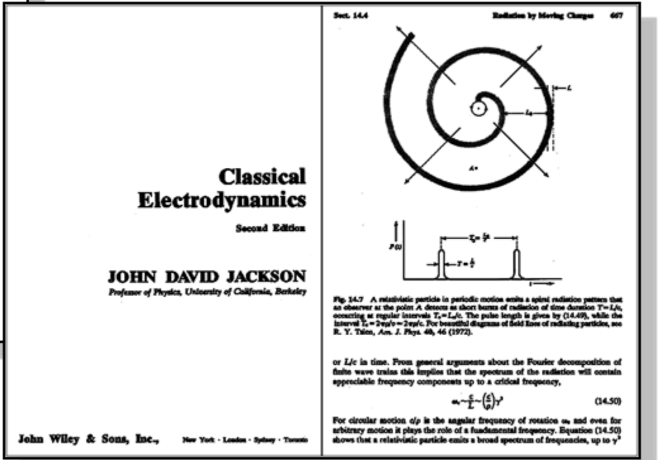

Classical Electrodynamics

Second Edition

JOHN DAVID JACKSON

Professor of Physics, University of California, Berkeley

John Wiley & Sons, Inc., New York · London · Sydney · Toronto

Sect. 14.4 Radiation by Moving Charges 667

Fig. 14.7 A relativistic particle in periodic motion emits a spiral radiation pattern that an observer at the point A detects as short bursts of radiation of time duration $T \sim L/c$, occurring at regular intervals $T_b = L_b/c$. The pulse length is given by (14.49), while the interval $T_b = 2\pi\rho/v \approx 2\pi\rho/c$. For beautiful diagrams of field lines of radiating particles, see R. Y. Tsien, *Am. J. Phys.* 40, 46 (1972).

or L/c in time. From general arguments about the Fourier decomposition of finite wave trains this implies that the spectrum of the radiation will contain appreciable frequency components up to a critical frequency,

$$\omega_c \sim \frac{c}{L} \sim \left(\frac{c}{\rho}\right)\gamma^3 \qquad (14.50)$$

For circular motion c/ρ is the angular frequency of rotation ω_0 and even for arbitrary motion it plays the role of a fundamental frequency. Equation (14.50) shows that a relativistic particle emits a broad spectrum of frequencies, up to γ^3

T.Esirkepov, SVB, K.Nishihara, T.Tajima, PRL (2004)

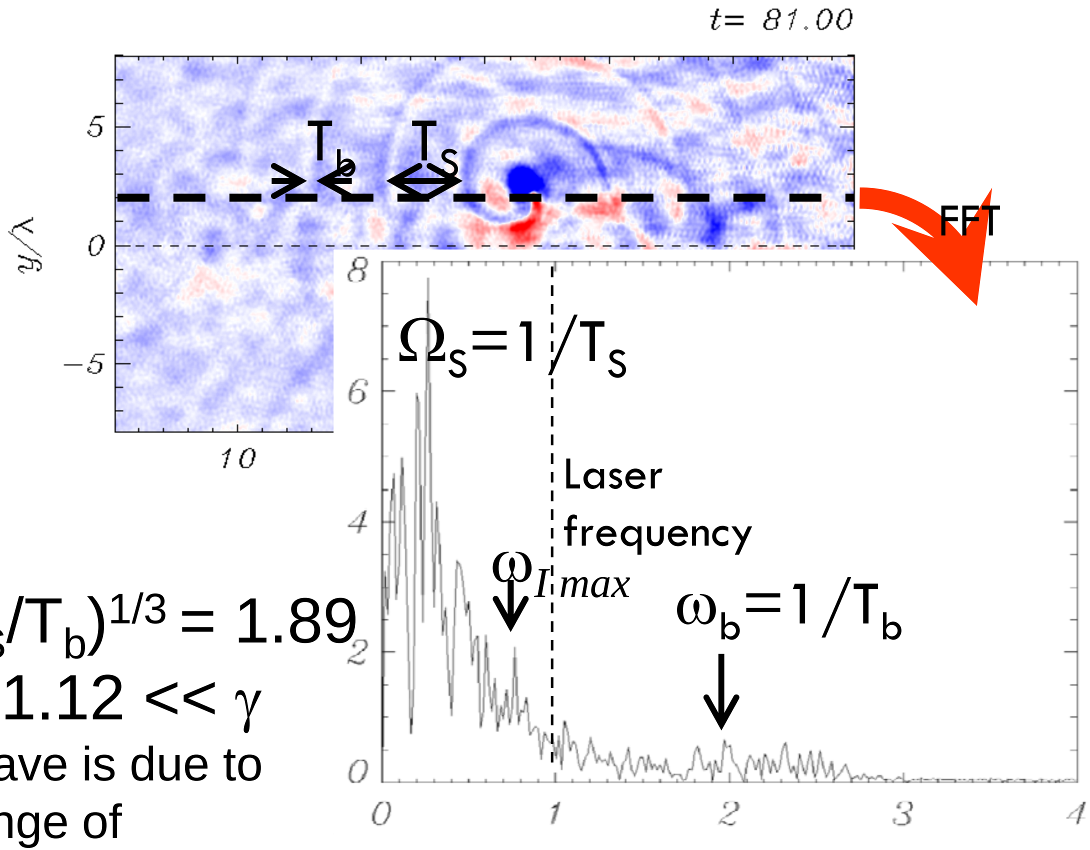

$\gamma \approx (T_S/T_b)^{1/3} = 1.89$

$\gamma_{e\ max}=1.12 << \gamma$

Spiral wave is due to fast change of electric charge density!

The solitons as the relativistic rotators can model the pulsar radiation under the earth laboratory conditions

5. Flying Mirror for Femto-, Atto-, … Super Strong Field Science

Kagami 鏡

("mirror" in Japanese)

Flying Mirror Concept

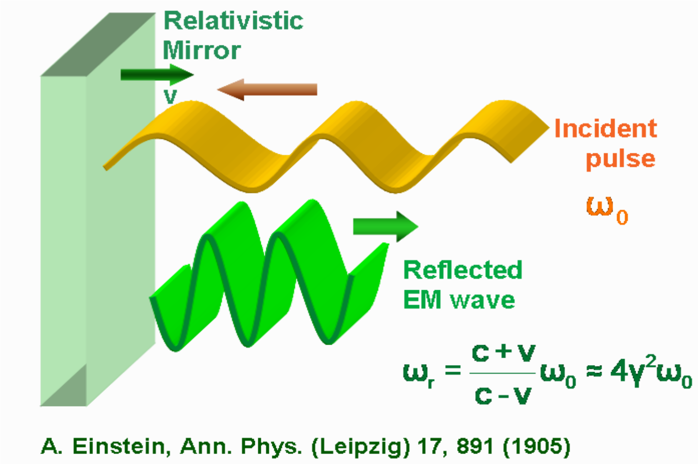

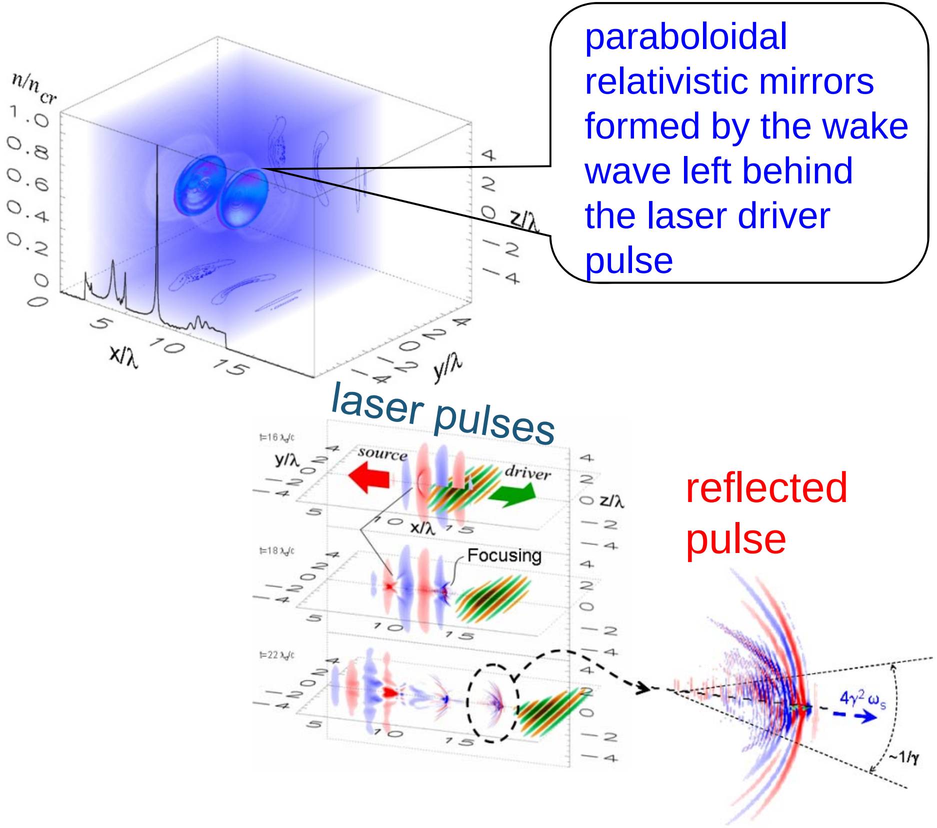

Frequency up-shifting and intensification of the light reflected at the relativistic mirror

S. Bulanov, T. Esirkepov, T. Tajima, Phys. Rev. Lett. 91, 085001 (2003)

Laser Energy & Power to Achieve the Schwinger Field

The driver and source must carry 10 kJ and 30 J, respectively

Reflected intensity can approach the Schwinger limit $I_{QED} = 10^{29} W / cm^2$

$$E_{QED} = \frac{m_e^2 c^3}{e\hbar}$$

It becomes possible to investigate such the fundamental problems of nowadays physics, as e.g. the electron-positron pair creation in vacuum and the photon-photon scattering

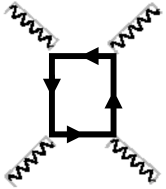

$$\mathcal{L} = \frac{1}{16\pi} F_{\alpha\beta} F^{\alpha\beta} - \frac{\kappa}{64\pi}\left[5\left(F_{\alpha\beta}F^{\alpha\beta}\right)^2 - 14 F_{\alpha\beta}F^{\beta\gamma}F_{\gamma\delta}F^{\delta\mu}\right]$$

The critical power for nonlinear vacuum effects is $\mathcal{P}_{cr} = \frac{45\pi^2}{\alpha} \frac{c E_{QED}^2 \lambda^2}{4\pi}$

$$\mathcal{P}_{cr} \approx 2.5 \times 10^{24} W$$

Light compression and focusing with the FLYING MIRRORS yields $\mathcal{P} = \mathcal{P}_0 \gamma_{ph}$

for $\lambda_0 = 1 \mu m$ $\lambda = \lambda_0 / 4\gamma_{ph}^2$ **with** $\gamma_{ph} \approx 30$ **the driver power**

P_{cr}=10 PW

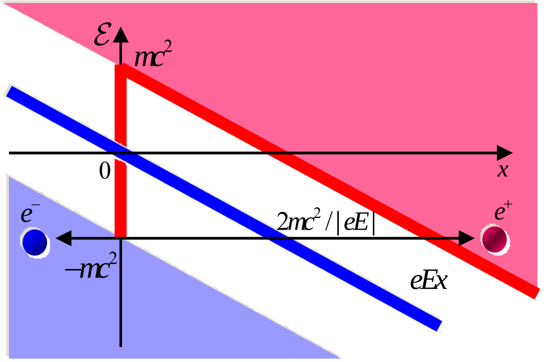

$$w = \frac{1}{\pi^2}\frac{\alpha c}{\lambda\!\!\!^{-}{}_c^{\,4}}\left(\frac{E}{E_{Schw}}\right)^2 \exp\left(-\frac{\pi E_{Schw}}{E}\right)$$

$$E \ll E_{Schw}, \quad \alpha = \frac{e^2}{\hbar c}, \quad \lambda\!\!\!^{-}{}_c = \frac{\hbar}{m_e c}$$

W.Heisenberg, H.Euler (1936)
J. Schwinger (1951)
Brezin, Itzykson (1970)
V.S.Popov (2001)

Pair production by two colliding pulses

S.S. Bulanov, N.B. Narozhny, V.S. Popov, V.D. Mur,), ZhETF 129, 14 (2006)

$I, W/cm^2$	E_0/E_S	N_e $\Delta=0.1$	N_e $\Delta=0.05$	N_h $\Delta=0.1$
$1.0\cdot10^{26}$	$2.5\cdot10^{-2}$	$4.5\cdot10^{-12}$	$6.0\cdot10^{-9}$	$7.1\cdot10^{-13}$
$2.0\cdot10^{26}$	$3.6\cdot10^{-2}$	$5.1\cdot10^{-2}$	7.2	$1.8\cdot10^{-2}$
$2.5\cdot10^{26}$	$4.0\cdot10^{-2}$	14 !!	$1.2\cdot10^{3}$	6.0
$5.0\cdot10^{26}$	$5.7\cdot10^{-2}$	$2.6\cdot10^{7}$	$5.5\cdot10^{8}$	$1.8\cdot10^{7}$

1. The effect becomes observable at $I \approx 10^{26} W/cm^2$
2. Small difference between e- and h-pulses

Courtesy of N.B.Narozhny

Proof of Principle Experiment

In our experiments, narrow band XUV generation was demonstrated

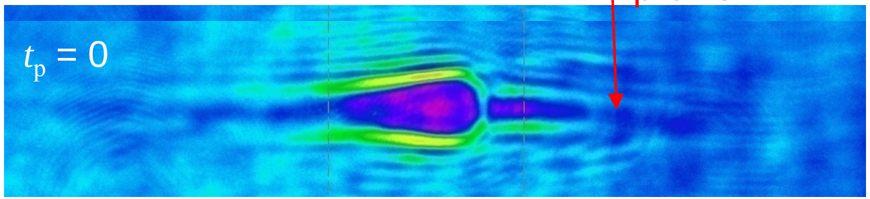

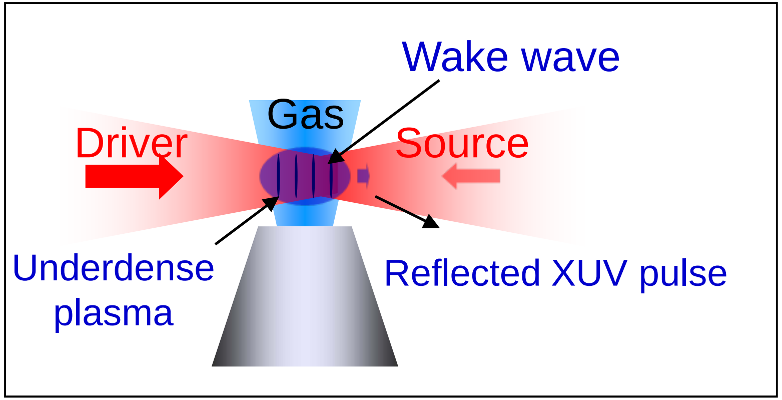

Detected signals

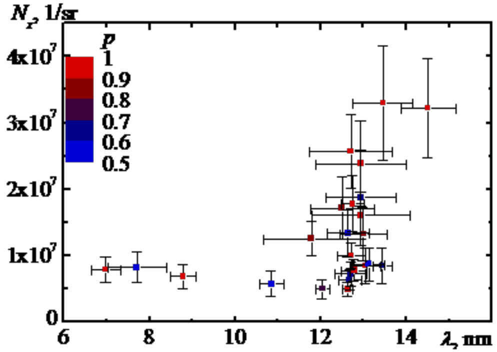

Frequency multiplication

$$\frac{\omega_r}{\omega_s} = 55 \ldots 114$$

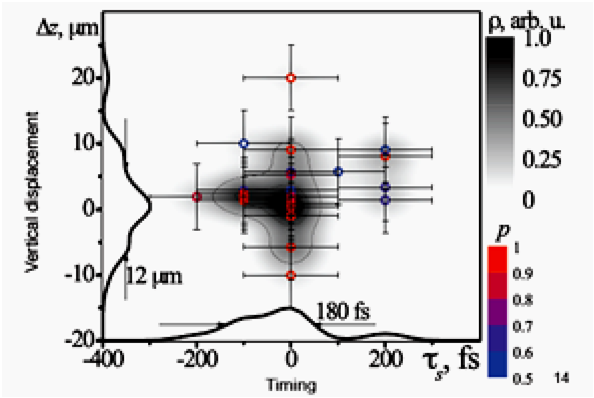

M. Kando, et al., Phys. Rev. Lett. 99, 135001 (2007);
A. Pirozhkov, et al., Phys. Plasmas 14, 123106 (2007)

6. Overdense Accelerating Mirror

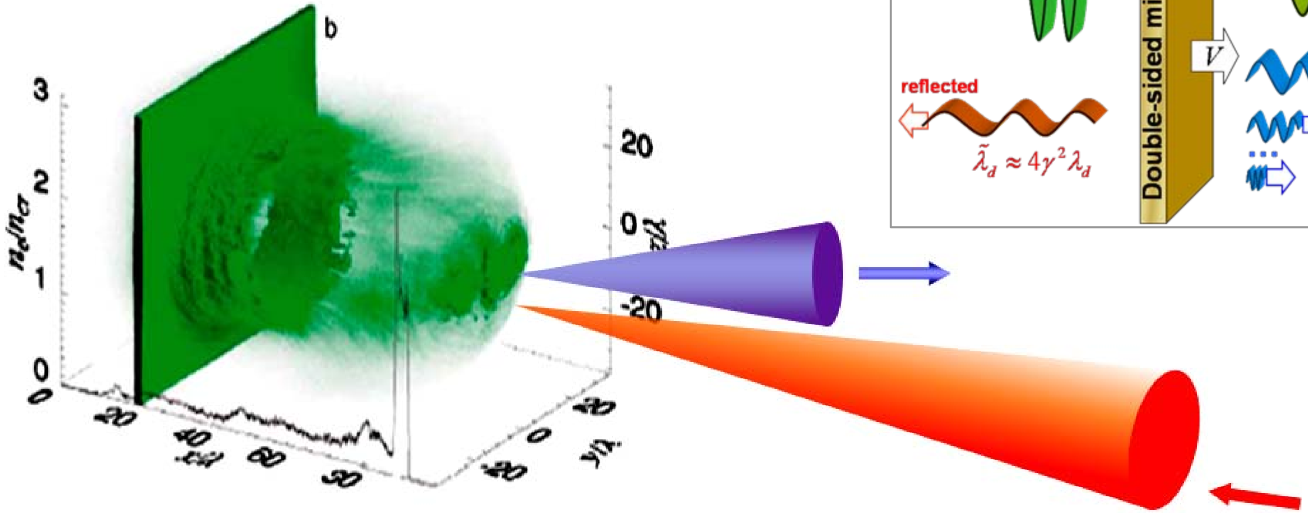

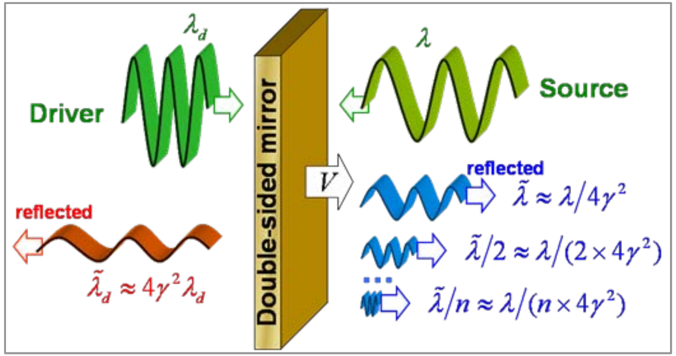

T.Esirkepov, et al. Phys. Rev. Lett. (2009) in press

Accelerating Double-Sided Mirror: Boosted HOH

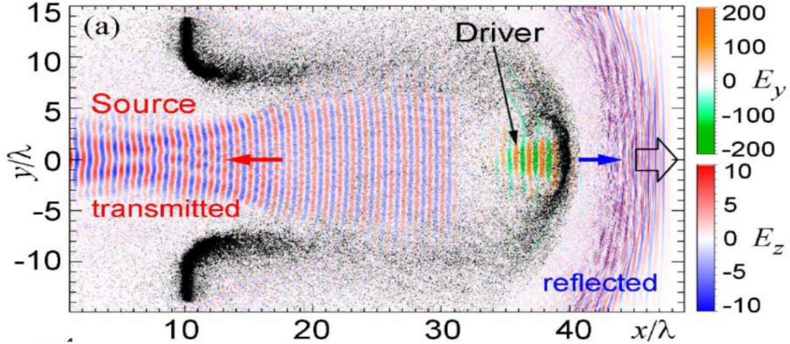

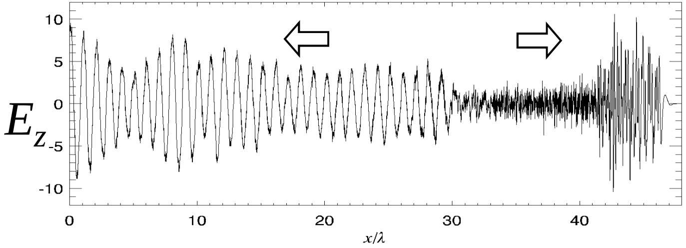

Reflected cycles

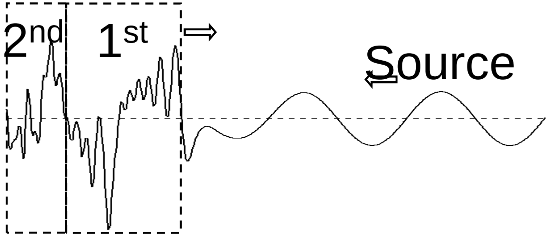

Field along x-axis

Spectrum at fixed time

$$I_\omega(t) = \int_{-\infty}^{+\infty} E_z(\tau) e^{-i\tau\omega - c^2(\tau - t)^2/\lambda^2} d\tau$$

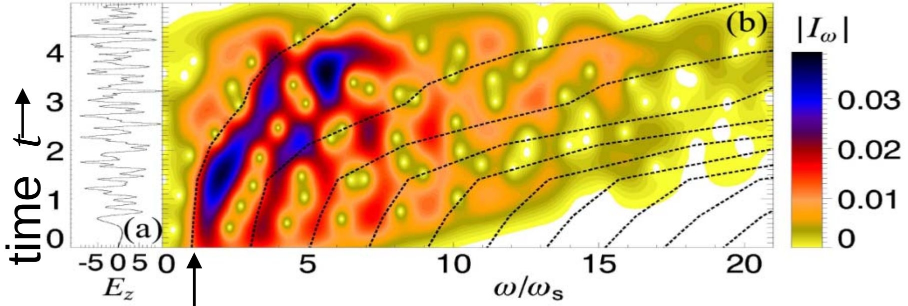

Dashed curves: $\frac{1+\beta(\tau)}{1-\beta(\tau)}\omega_0 \times (2n-1), \quad n = 1, 2, 3\ldots$

τ – time of emission

time of detection: $t = \tau - \int_0^\tau \beta(\tau) d\tau$

Reflected light structure:

- Fundamental mode $\times 4\gamma^2$
- High harmonics $\times 4\gamma^2$
- Shift due to acceleration

7. Applications

Such X-ray sources are expected for applications and for fundamental science.

a) biology and medicine - single-shot X-ray imaging in a ‘water window’ or shorter wavelength range.

b) atomic physics and spectroscopy – the multi-photon ionization & high Z hollow atoms (and ions).

c) probing relativistic plasmas, for the nonlinear wave theory

& for charged particle acceleration

d) novel regimes of soft X ray - matter interaction: dominant radiation friction & quantum physics cooperative phenomena.

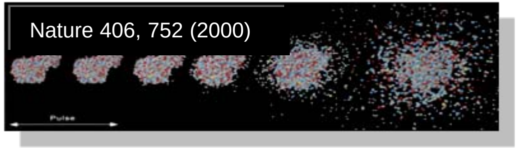

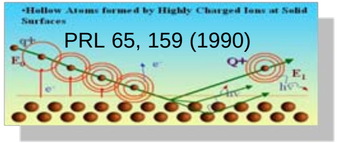

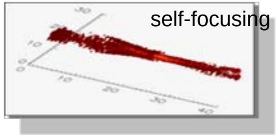

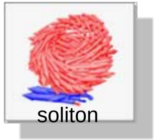

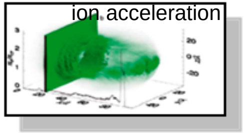

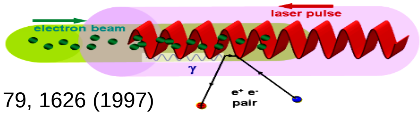

PRL 79, 1626 (1997)

High Field Science

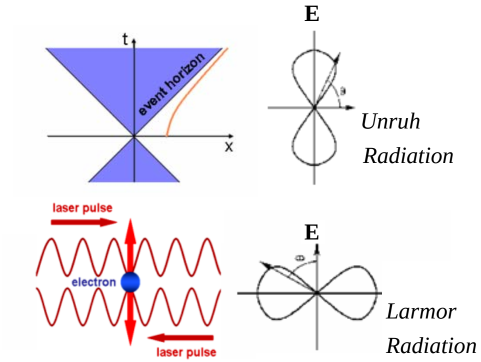

Unruh radiation (Chen&Tajima (1999))

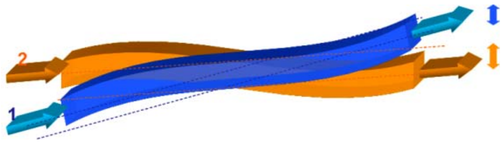

Birefringent e.m. vacuum (Rosanov (1993))

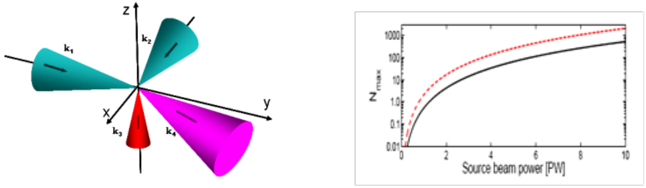

4-wave mixing (Lundström et al (2006))

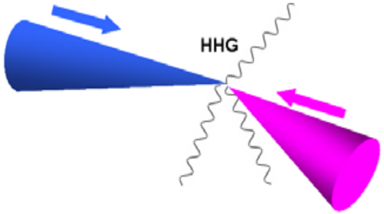

Higher harmonic generation through quantum vacuum interaction (Fedotov & Narozhny (2006); Di Piazza, Keitel)

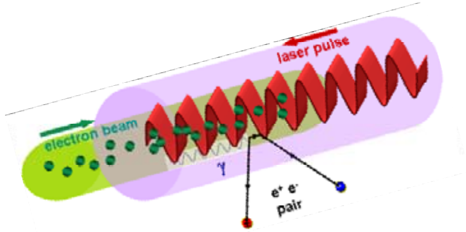

Electron-positron pair production in the laser interaction with the electron beam: $e^- + n\gamma \rightarrow \gamma, \gamma + n\gamma' \rightarrow e^+ + e^-$
Bula et al (1996); Burke et al (1997)

8. Conclusion

a) Ultra Short Pulse Laser – Matter Interaction has entered the Ultrarelativistic Regime. By this it has opened a new field of Relativistic Laboratory Astrophysics

b) Laser Piston+Flying Mirror+Oscillating Mirror will provide in a nearest future the instruments for nonlinear vacuum probing and for studying other fundamental problems

Laser-Plasma Interaction in the "Radiation-Dominant" Regime

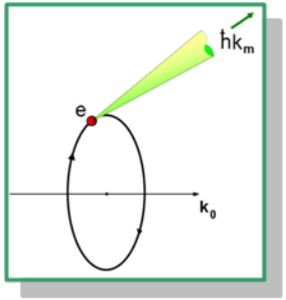

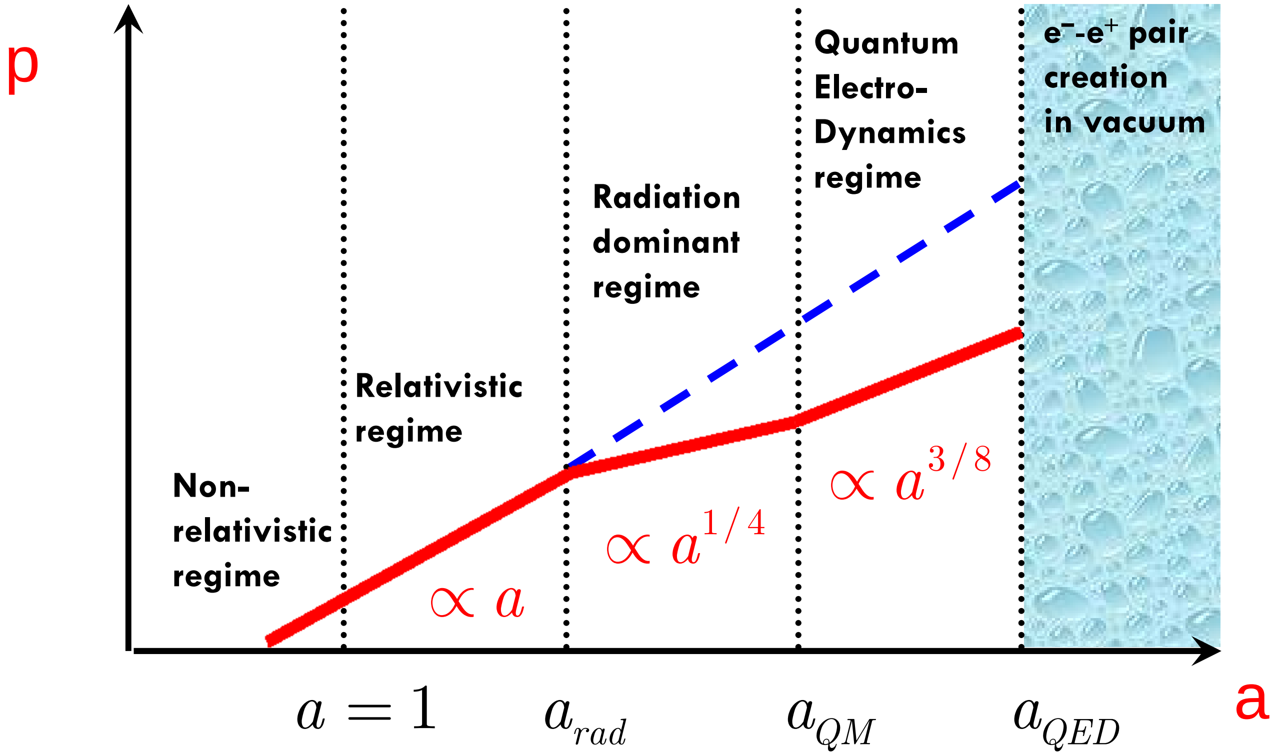

2D case: The field-line equation reads

$$\frac{dx}{B_x} = \frac{dy}{B_y} = ds$$

Using the relationships

$$B_x = \partial_y A_z - \partial_x F, \quad B_y = -\partial_x A_z - \partial_y F,$$

introducing complex variable $\varsigma = x + iy$, complex field and potential

$$B = B_x - iB_y, \quad \Phi = F - iA_z,$$

we obtain the Hamiltonian equations for the magnetic field lines $(' = d/ds)$:

$$\varsigma' = -\frac{\partial \Phi}{\partial \varsigma}$$

The magnetic field lines are on the surfaces $A_z =$ constant

E.M. field energy density

Energy loss by radiation

$$-\frac{d\mathcal{E}}{dt} = \frac{2e^2}{3c} N^2 \omega_0^2 \gamma^2 \left(\gamma^2 - 1\right)$$

Frequency distribution of the total energy emitted by coherently rotating electrons

$$\frac{dI}{d\omega} = \sqrt{3} N^2 \gamma \frac{e^2}{c} \frac{2\omega}{3\gamma^3 \omega_0} \int_{\frac{2\omega}{3\gamma^3\omega_0}}^{\infty} K_{5/3}(\xi) d\xi$$

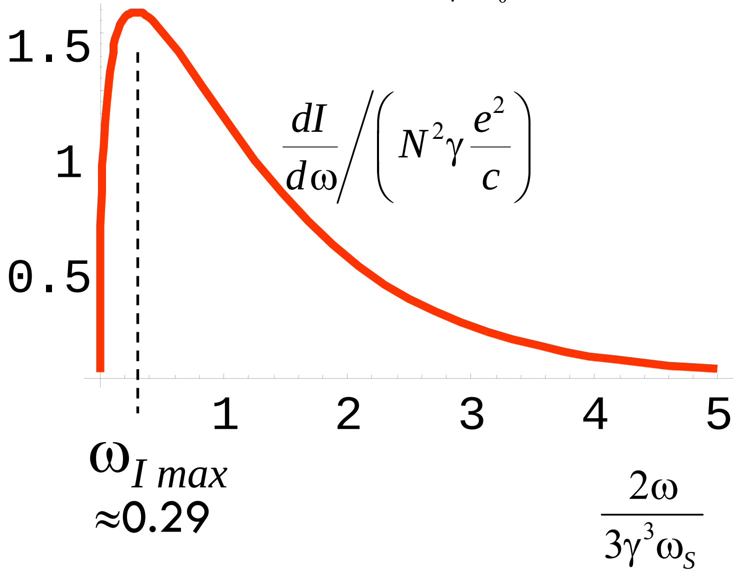

Compact Coherent Ultrafast X-Ray Source

X-ray source	Wavelength	Pulse Duration	Pulse Energy	Mono-chromaticity (Δλ/λ)	Coherence
XFEL (DESY)	13.8 nm	50 fs	100 μJ	10^{-3}	spatial good
Plasma XRL	13.9 nm	7 ps	10 μJ	10^{-4}	spatial good
Laser plasma	wide spectrum 1 nm – 40 nm	1 ps – 1 ns	10 μJ	10^{-2} – 10^{-3}	No
HHG	5 – 200 nm	100 attosec	1 μJ	10^{-2} – 10^{-3}	spatial and temporal good
Flying Mirror	0.1 – 20 nm	< 1 fs	1 mJ	10^{-2} – 10^{-4}	spatial and temporal good

Predicted by the FM theory parameters of the x-ray pulse compared with the parameters of high power x-ray generated by other sources

Brightness

$$B = 2\times10^{28}\left(\frac{\mathcal{E}_{las}}{1\,\mathrm{J}}\right)\sqrt{\frac{1\,\mathrm{KeV}}{\hbar\omega_\gamma}}\;\frac{1}{\mathrm{mm}^2\,\mathrm{mrad}^2\,0.1\%\,\mathrm{bandwidth}}$$

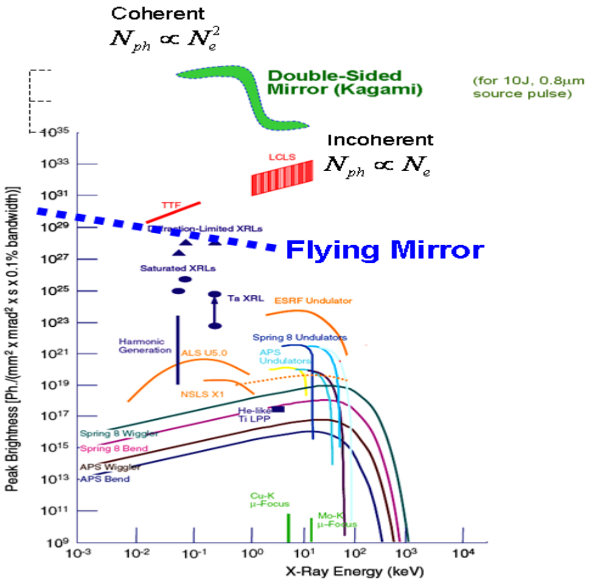

Peak brightness of various light sources

Flying Mirror in the Head-On Collision Experiment

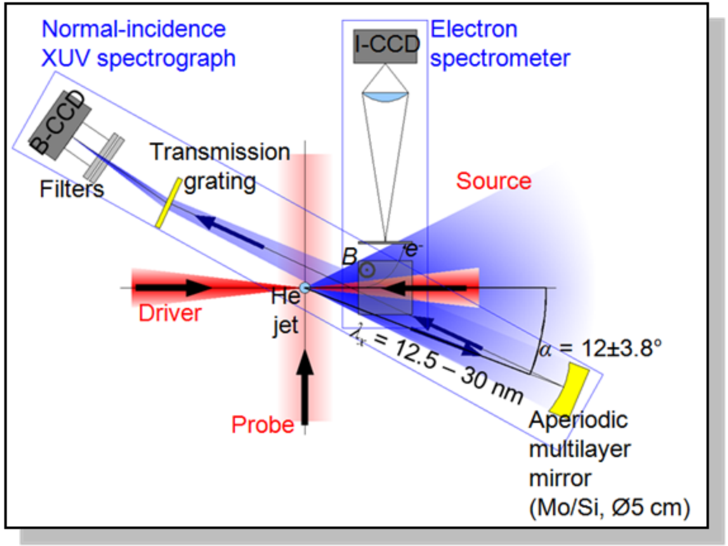

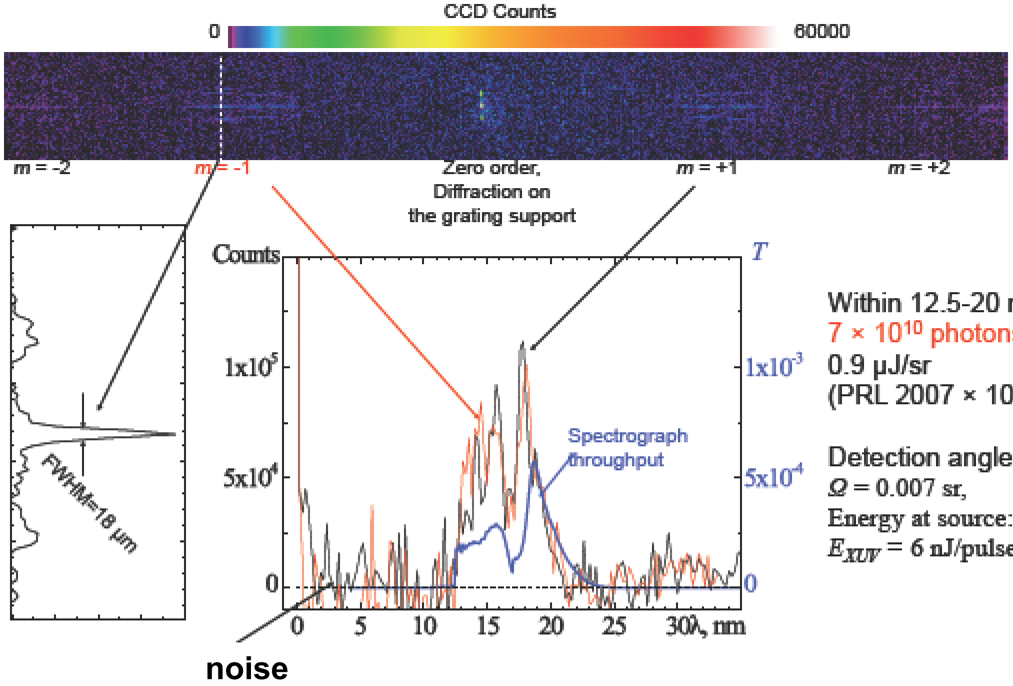

Within 12.5-20 nm:
7×10^{10} photons/sr
0.9 µJ/sr
(PRL 2007 × 1000)

Detection angle:
Ω = 0.007 sr,
Energy at source:
E_{XUV} = 6 nJ/pulse

Two head-on colliding laser pulses